

Distortion of sonic bangs by atmospheric turbulence

By S. C. CROW†

National Physical Laboratory, Teddington, England

(Received 10 June 1968 and in revised form 4 October 1968)

Recorded pressure signatures of supersonic aircraft often show intense, spiky perturbations superimposed on a basic *N*-shaped pattern. A first-order scattering theory, incorporating both inertial and thermal interactions, is developed to explain the spikes. Scattering from a weak shock is studied first. The solution of the scattering equation is derived as a sum of three terms: a phase shift corresponding to the singularity found by Lighthill; a small local compression or rarefaction; a surface integral over a paraboloid of dependence, whose focus is the observation point and whose directrix is the shock. The solution is found to degenerate at the shock into the result given by ray acoustics, and the surface integral is identified with the scattered waves that make up the spikes. The solution is generalized for arbitrary wave-forms by means of a superposition integral. Eddies in the Kolmogorov inertial subrange are found to be the main source of spikes, and Kolmogorov's similarity theory is used to show that, for almost all times t after a sonic-bang shock passes an observation point, the mean-square pressure perturbation equals $(\Delta p)^2 (t_c/t)^{\frac{7}{2}}$, where Δp is the pressure jump across the shock and t_c is a critical time predicted in terms of meteorological conditions. For an idealized model of the atmospheric boundary layer, t_c is calculated to be about 1 ms, a figure consistent with the qualitative data currently available. The mean-square pressure perturbation just behind the shock itself is found to be finite but enormous, according to first-order scattering theory. It is conjectured that a second-order theory might explain the shock thickening that actually occurs.

1. Introduction

The passage of a distant supersonic aircraft is marked by a sonic bang, so called because the pressure waves excited at successive instants by the motion of the aircraft crowd against an envelope and combine into a wave of great intensity and brevity. In the case of steady and level flight, the envelope is the Mach cone originating near the nose of the aircraft (the term Mach cone is being used rather loosely here, but it is good enough for descriptive purposes). The pressure field near the aircraft may have a complicated structure comprising alternate shocks and expansion waves, as shown in figure 1(*a*), but Whitham (1952, 1956) discovered that the field attains a simple and universal form at great distances from the aircraft. The waves merge and attenuate as they propagate outward, until

† Present address: Boeing Scientific Research Laboratories, Seattle, Washington.

eventually a single expansion wave remains, sandwiched between two shocks. Viewed from a distance comparable to the altitude of the aircraft, the Mach cone appears as a thin conical shell, whose surfaces are the leading and trailing shocks. The shell thickness is depicted with great exaggeration in figure 1 (b). Whitham showed that the two shocks have equal strengths, that the expansion between them is uniform, and that they separate as the one-fourth power of distance from the aircraft. For the case of homogeneous and still air, he provided formulae for calculating the strength and separation of the shocks at any point on the Mach cone in terms of the shape of the aircraft. Subsequent workers, using the approximations of ray acoustics, generalized the formulae to allow for non-steady flight

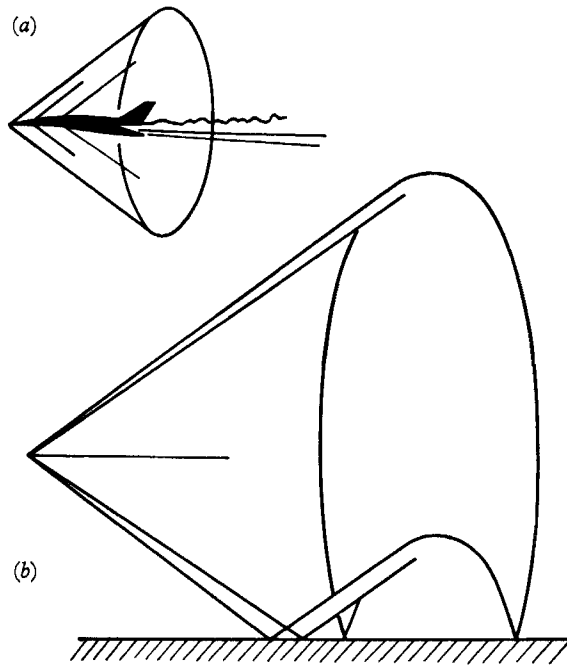


FIGURE 1. The Mach cone: (a) viewed close to the airplane; (b) viewed from a distance comparable to the altitude of the airplane. (b) Shows the reflexion from the ground and the finite thickness of the conical shell (greatly exaggerated).

(Lansing 1964), for refraction of the Mach cone in temperature gradients (Warren 1965), and for convection of the Mach cone in winds (Friedman, Kane & Sigalla 1963). Lilley (1965) presented a review of the comprehensive theory.

The pressure signature of a supersonic aircraft is shaped like an *N*, according to Whitham's theory, provided the craft is flying high enough for the asymptotic wave-form to be realized. Figure 2 represents the kind of signature that is predicted theoretically: $p(t)$ is the history of the net pressure at an observation point fixed on the ground, and p_0 is the ambient pressure. The difference $p(t) - p_0$ is heard as a sonic bang. Any point on the ground eventually receives a sonic bang if the Mach cone is not refracted upward by thermal gradients or winds. In the absence of such refractive effects, the cone intersects the ground in a broad

hyperbola and reflects upward along the intersection as shown in figure 1(b). Figure 2 can be regarded as applying to a point on the ground where the bang is loudest—directly under the flight path of the aircraft. The pressure at the ground includes contributions from both incident and reflected waves and is double the pressure of the incident wave alone. The doubled pressure jump across the shocks will be 1.5–2.5 lb./ft.² for the supersonic transports of the immediate future, and the separation between the shocks will be 200–300 ft. The speed of sound is about 1000 ft./s at sea level, so the duration of the *N*-wave will be 200–300 ms. Those estimates set the scales in figure 2.†

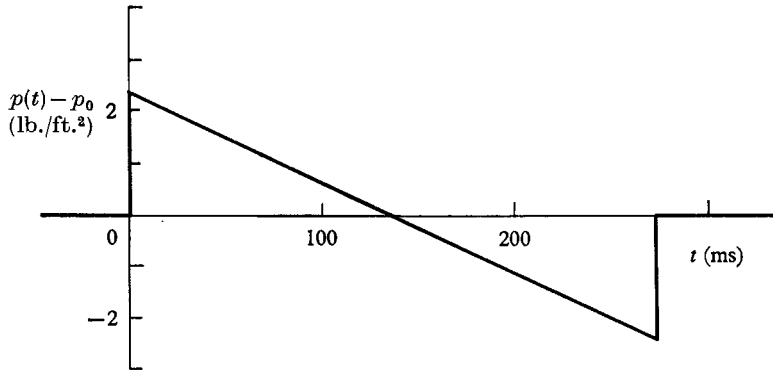


FIGURE 2. A typical theoretically predicted *N*-wave from a supersonic transport.

By 1964, when detailed pressure signatures were recorded during supersonic flights over Oklahoma City in the United States, the theory of sonic bangs appeared tolerably complete. Kane & Palmer (1964) presented a comparison between the experimental data and Whitham's theory. Similar data were obtained during Exercise Westminster in the United Kingdom (Webb & Warren 1965). The most recent and extensive tests have been carried out over Edwards Air Force Base in the United States (Garrick & Maglieri 1968). All the data show that Whitham's theory correctly predicts the large-scale features of sonic bangs: they are *N*-shaped whenever the theory predicts that they should be, and they have about the right amplitude and duration. Often, however, a high-pitched spiky fine structure is superimposed on the basic *N*-shape. The pressure excursions can be positive or negative, and those immediately behind the shocks tend to be especially large. As a consequence, three types of *N*-wave have been distinguished in the literature and are shown in figure 3: (a) peaked, which corresponds to a positive shock spike; (b) rounded, corresponding to a negative shock spike; (c) normal, corresponding to a shock spike that happens to be untypically small.

† It should be noted that the supersonic transports will be so large that the asymptotic wave-form may *not* always be realized: shocks generated midway along the fuselage may not coalesce with the leading shock before the wave reaches the ground (Carlson 1967). The resulting pressure signature would not be a clean *N*, but the difference has no bearing on the discussion of this paper, and the *N*-shape is retained in the figures for clarity.

The impulse of the fine structure is much less than the impulse of the basic N , so the spikes will impose negligible loads on window panes and such. The fine structure nevertheless may have an important bearing on the psychological impact of a sonic bang. The reason has to do with the physiology of hearing (Johnson & Robinson 1967). The ear and its associated nervous system can be regarded crudely as a series of oscillators tuned to $\frac{1}{3}$ octave bands in the frequency range 20–20 000 c/s. All the oscillators respond to an instantaneous pressure rise like the leading shock of an undeformed N -wave, but those tuned to high

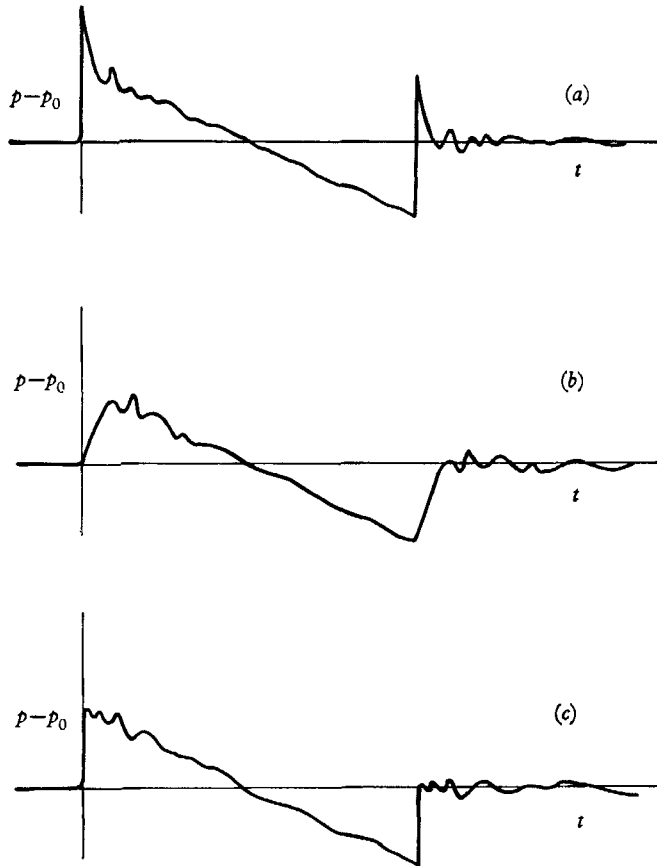


FIGURE 3. Typical recorded sonic-bang pressure histories: (a) peaked; (b) rounded; (c) normal.

frequencies are excited only weakly. The high-pitched spikes that characterize deformed N -waves would have little effect on oscillators tuned to frequencies below, say, 100 c/s, but they could force higher-frequency oscillators much more violently than a simple jump would have done. A given energy imparted at a higher frequency is amplified by the nervous system into a much louder and more startling sound than the same energy imparted at a low frequency, so high-pitched spikes containing relatively little acoustic energy could considerably increase the objectionable quality of a sonic bang.

Five curious attributes are clues to the origin of the experimentally observed fine structure:

(1) Perturbations from the basic N -shape are random. The spikes fluctuate rapidly as the N -wave passes from point to point along the ground, and they take on either sign regardless of the direction of the wind or the thermal gradient (Garrick & Maglieri 1968).

(2) The amplitude of the pressure perturbation at the leading or trailing shock tends to be large, often comparable to the pressure jump that would have occurred across an undeformed shock. The amplitude of the perturbations decreases rapidly behind the shock.

(3) The duration of the spike behind a shock is very short, say 5–30 ms, corresponding to a length scale in the incident pressure wave of 5–30 ft. (the length scale is the speed of sound times the duration measured at a fixed point; the speed of the aircraft is irrelevant, because the spiky structure is not convected rigidly over the ground). The duration and the length scale of the spikes increase steadily behind the shock (figure 3), but the duration of a spike is never more than a fraction of the total duration of the N -wave.

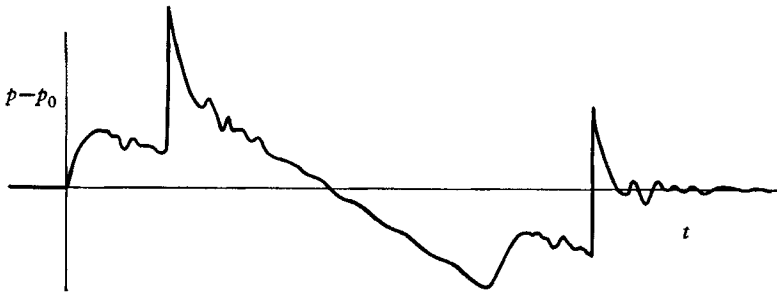


FIGURE 4. Pressure history recorded from a microphone 50 ft. or so above the ground.

(4) The perturbations associated with the leading shock are exactly the same as those associated with the trailing shock (Kane & Palmer 1964). If the leading shock is peaked, then the trailing shock is peaked, and so on.

(5) In the course of Exercise Westminster, microphones were located not only on the ground, where pressure signatures of the kind shown in figure 3 were recorded, but also on masts at distances 30–50 ft. above the ground. Above the ground there is a time delay between the incident and reflected waves, and the pressure history has a more complex shape, of which figure 4 is an example (cf. Webb & Warren 1965, figures 7, 15, etc.). The first and third shocks from the left are the leading and trailing shocks of the incident wave, and the second and fourth shocks are associated with the reflected wave. The perturbations associated with the leading and trailing shocks of the incident wave are the same. The perturbations associated with the two shocks of the reflected wave are also the same as each other, but they often bear little resemblance to the perturbations associated with the incident N -wave. Figure 4 shows such a disparity.

At first glance those five attributes seem paradoxical. Attribute (1) strongly suggests that random eddies or temperature inhomogeneities distort the N -wave as it propagates through atmospheric turbulence on its way from the aircraft to the ground. That conclusion is consistent with attribute (4), since the turbulence is certainly 'frozen' during the 200 ms passage time of the N -wave. If turbulence does distort the N -wave, on the other hand, it seems strange that the *mean* winds and temperature gradients fail to impose a significant average distortion. The mean wind is almost always much stronger than turbulent velocity fluctuations, and in any case the acoustic effects of turbulence are usually very small, being proportional to some power of a typical fluctuation Mach number. The Mach number of atmospheric turbulence, which is confined mostly to a surface layer 1000–3000 ft. thick, is rarely greater than 1/200 under ordinary meteorological conditions (Lumley & Panofsky 1964, chapter 4). One would therefore expect the perturbations due to turbulence to be very small, in contradiction with attribute (2). According to attribute (3), moreover, the length scale of the random spikes in the pressure signature is many times smaller than the average scale of the energy-bearing eddies in the atmospheric boundary layer. Finally, attribute (5) suggests the puzzling (and erroneous) conclusion that only disturbances in the first 50 ft. above the ground are responsible for the distortion. Large-scale, weakly compressible turbulence appears not only to produce a fine-scale, high-amplitude distortion, but to do so in the lowest stratum of the boundary layer.

The paradox is only apparent. Acoustic scattering theory, studied by Lighthill (1953) and others, is applied in the following sections to explain the five attributes listed above. All strata of the atmospheric boundary layer contribute to the scattering, and eddies in the Kolmogorov inertial subrange, rather than the energy-bearing eddies, are the primary source of N -wave spikes. The assumptions of local isotropy and of similarity in the inertial subrange permit a quantitative and realistic statistical description of the distortions.

2. Inertial and thermal scattering

In order to apply scattering theory to the sonic-bang problem without undue complication, it is necessary to make a basic assumption about the location of the turbulence that distorts the N -wave. The turbulence is assumed to be concentrated near the ground in a boundary layer of thickness much less than the altitude of the aircraft and also much less than the scale height of the atmosphere. The cruising altitude of the supersonic transports will be above 50,000 ft., the scale height of the atmosphere is 30,000 ft., and the thickness of the atmospheric boundary layer is likely to be 3000 ft. or less (Zilitinkevich, Laikhtman & Monin 1967; Lumley & Panofsky 1964, pp. 74–75). This first assumption therefore will be strongly satisfied, except perhaps in unusual cases when the N -wave descends through towering cumulus clouds or through a jet stream surrounded by intense clear-air turbulence. Those cases are excluded from the analysis. An immediate consequence of the assumption is that gravitational variations in the ambient pressure and density of the air, which are significant over altitudes comparable to the scale height, can be neglected throughout the thin scattering region.

A second consequence is that all the scattering occurs far from the aircraft, in a region where the N -wave is weak. A third consequence is that the curvature of the Mach cone (figure 1) is negligible in the scattering region. A patch of the conical shell can be regarded as a wave travelling in a direction normal to the shock fronts, away from its point of origin on the flight path of the aircraft. As it passes through the scattering region in the last several seconds of its journey from the aircraft to the ground, the patch behaves as a plane acoustic wave. The effect of non-linear steepening, which causes the wave to develop an N -shape as it travels from the aircraft to the scattering region, has no time to alter its shape further. † Random fluctuations in the boundary layer cause the final distortions, which appear as spikes in the pressure history recorded on the ground.

If the pressure distortions are sufficiently weak, they can be treated as secondary waves scattered from the incident N -wave as it interacts with fluctuations in the turbulent boundary layer. It is then possible to write the net pressure excursion $p - p_0$ as the sum of an incident pressure wave p^N satisfying the homogeneous wave equation and a scattered wave p^S forced by the interaction between the incident wave and the fluctuations:

$$p - p_0 = p^N + p^S.$$

The assumption that $p^N \gg p^S$ is a second major restriction on the analysis. This second assumption is sometimes violated in practice as figure 3 shows, but the resulting theory correctly accounts for the origin of N -wave distortions, if not for their subsequent interaction with the background turbulence. Neglect of such 'second scattering' results in a tractable first-order scattering theory.

Two kinds of fluctuation cause scattering: momentum fluctuations associated with the eddy motion, and thermal fluctuations due to convective heating from the ground. The two kinds of scattering, which may be called inertial scattering and thermal scattering, are discussed at length in a lucid review by Batchelor (1957).

A treatment of inertial scattering involves splitting the net velocity into a rotational field u_i associated with the atmospheric turbulence and an acoustic field v_i associated with the N -wave. As the N -wave passes an eddy, the local momentum flux changes by an amount $\rho(u_i v_j + u_j v_i)$, where ρ is the density. The local pressure changes accordingly, and the pressure change then radiates away as an acoustic wave. Since atmospheric eddies swirl at very low Mach numbers, the turbulent field u_i can be taken as incompressible, and the local density ρ can be replaced with its ambient value ρ_0 in the expression for the momentum flux change.

The connexion between thermal fluctuations and scattering is somewhat less direct. Suppose that convection of heat from the ground causes the local temperature T to depart by an amount θ from its ambient value T_0 . The temperature fluctuations θ in turn give rise to inhomogeneities in density and speed of sound,

† This assertion needs to be qualified for regions immediately behind the N -wave shocks. Acoustic waves following a shock tend to gain on the shock and disappear into it (Lighthill 1956). For every lb./ft.² of its strength, a weak shock in air consumes about 0.25 ft./s of a trailing wave pattern. Non-linear steepening is likely to dominate scattered waves arriving in the first 1–2 ms after the passage of a shock but to have little effect on those arriving subsequently.

the properties of a medium relevant to acoustic wave propagation. The speed of sound c , for example, can be written as the sum of its ambient value c_0 and a thermally induced fluctuation c_θ . Thermally induced changes in density and speed of sound are not independent. The heated air is free to expand, so the pressure cannot depend directly on θ . For a nearly perfect gas like air, the combination ρc^2 is proportional to pressure and is therefore independent of θ . Changes in ρ are related to c_θ and need not appear separately in the scattering equation. Thermally scattered waves arise as fluctuations in the speed of sound accelerate or retard the advancing N -wave.

The comprehensive wave equation that describes both inertial and thermal scattering, namely

$$\left\{ \frac{1}{c_0^2} \frac{\partial^2}{\partial t^2} - \nabla^2 \right\} p^S = \frac{\partial}{\partial x_i} \left\{ 2\rho_0 u_j \frac{\partial v_i^N}{\partial x_j} + 2 \frac{c_\theta}{c_0} \frac{\partial p^N}{\partial x_i} \right\}, \quad (2.1)$$

is the starting-point of this investigation. Equation (2.1) follows from equations (25) and (45) in the review by Batchelor (1957) and is derived from the fundamental equations of motion in an earlier version of this paper (Crow 1968). Equation (2.1) has the expected form of an inhomogeneous wave equation for p^S . The forcing function on the right-hand side couples inertial and thermal fluctuations to quantities, superscribed by N , associated with the undeformed N -wave. The incident pressure and velocity fields, p^N and v_i^N , are related to one another by the familiar equations of linear acoustics, and both obey the homogeneous wave equation. The scattered density and velocity fields corresponding to p^S are *not* related to p^S , inside the turbulent region, by the equations of linear acoustics, and they obey inhomogeneous wave equations somewhat more complicated than (2.1). The only scattered quantity of practical significance, of course, is p^S .

Much of the analysis in this paper concerns scattering from a weak shock. There are two reasons for concentrating on shocks. First, experimental pressure histories of the kind sketched in figure 3 indicate that only the perturbations arriving in the first 50 ms or so after the passage of either N -wave shock are likely to be important. It is reasonable to assume that those perturbations are associated with the sharp pressure rises across the shocks and are insensitive to the rate of expansion between them. For the purpose of computing the perturbation behind one shock, the other shock can safely be disregarded, and the rate of decrease of pressure between the two shocks can be taken as zero. To the extent that those approximations are valid, the solutions of the shock and N -wave problems are the same. Second, the solution of (2.1) for an incident shock is particularly simple and can be used as the kernel in a superposition integral to solve the general first-order scattering problem. The general solution for plane waves of arbitrary form is given near the end of § 3. Meanwhile, the incident wave is to be regarded as a single plane and weak shock, like the leading shock of an N -wave, descending obliquely through the scattering region at the ambient speed of sound.

It is convenient to choose a co-ordinate system x_i tilted with respect to the ground so that x_2 and x_3 are parallel to the shock and x_1 , which is written as x for short from now on, is perpendicular and increases toward the point where the aircraft originally sent out the shock (cf. figures 5 and 6). The origin $x_i = 0$ is

chosen to coincide with the fixed observation point where the pressure history is desired. Reflexion of the shock and the scattered waves at the ground can be neglected for the time being as though the observation point were suspended in mid-air; the reflected waves are taken into account by the method of images in § 5. If the origin of time is chosen so that the shock passes the observation point at $t = 0$, then the incident pressure wave travelling in the negative direction along the x -axis (i.e. the x_1 -axis) has the form

$$p^N = \Delta p H(x + c_0 t),$$

which of course is a solution of the homogeneous wave equation. H is the Heaviside unit step function, and Δp is the pressure jump across the shock in the absence of scattering. According to linear acoustics, $v_1^N = -p^N/\rho_0 c_0$, and the other components of v_i^N are zero. The scattering equation (2.1) thus assumes an extremely simple form,

$$\left\{ \nabla^2 - \frac{1}{c_0^2} \frac{\partial^2}{\partial t^2} \right\} s(\mathbf{x}, t) = \frac{\partial}{\partial x} \left\{ 2m(\mathbf{x}, t) \delta(x + c_0 t) \right\}, \quad (2.2)$$

in terms of two fundamental dimensionless quantities:

$$\begin{aligned} s &= p^S/\Delta p, & \text{the fractional pressure perturbation;} \\ m &= (u_1 - c_\theta)/c_0, & \text{an effective normal Mach number, representing the combined action of turbulent velocity fluctuations and temperature inhomogeneities.} \end{aligned}$$

$\delta(x + c_0 t)$ is a delta function travelling up the x -axis. Notice that the only component of turbulent velocity that contributes to scattering is the one normal to the shock and that normal velocity fluctuations and thermal fluctuations scatter in exactly the same fashion in a perfect gas, their combined action being represented by the effective normal Mach number $m(\mathbf{x}, t)$.

There is a second way of interpreting m that is worth considering. To first order in the small quantities u_1/c_0 and c_θ/c_0 ,

$$1 + m = c_0/(c - u_1). \quad (2.3)$$

The ratio $c_0/(c - u_1)$ is a generalized index of refraction, the ordinary index of refraction being c_0/c . The dimensionless quantity m therefore represents the departure of the generalized index of refraction from unity. That interpretation is used in § 4 to compare the results of scattering theory with the better-known but someways less general results of ray acoustics.

Because inertial and thermal scattering combine in such a simple way, it is possible to find the dimensionless pressure perturbation $s(0, t)$ at the observation point without considering which effect, if either, is dominant. In §§ 3–5, which concern the deterministic solution of (2.2) for a given scattering field $m(\mathbf{x}, t)$, no mention has to be made of the particular kind of scattering involved. A distinction between inertial and thermal scattering arises, however, during the statistical analysis of §§ 6–8: c_θ is a random scalar field and u_1 a component of a random vector field, so the two necessarily have somewhat different statistical characteristics. In order to investigate the relative strengths of inertial and thermal scattering, it is desirable to write m in yet a third way,

$$m = u_1/c_0 - \theta/2T_0, \quad (2.4)$$

where the fact that c^2 varies as T in a perfect gas has been used. As an order-of-magnitude estimate,

$$\frac{\text{thermal scattering}}{\text{inertial scattering}} \sim \frac{\theta/T_0}{u/c_0},$$

where u is a typical turbulent velocity fluctuation. Thermal scattering is most significant in a boundary layer driven entirely by buoyant convection. Kinetic energy gained from buoyant convection in such a boundary layer eventually cascades into successively finer scales of turbulence and is lost to viscous dissipation. On the average,

$$\frac{\text{buoyant production}}{\text{dissipation}} \sim \frac{ug\theta/T_0}{u^3/\delta} \sim 1$$

(Townsend 1957). The length scale of the eddies has been taken as some fraction of the thickness δ of the thermal boundary layer. Those two estimates together imply that

$$\frac{\text{thermal scattering}}{\text{inertial scattering}} \sim \left(\frac{u}{c_0}\right) \left(\frac{\Delta}{\delta}\right),$$

where Δ is the scale height c_0^2/g of the atmosphere. The ratio Δ/δ is likely to be 10 or 20, but the Mach number u/c_0 is never much more than $1/200$. Thermal scattering thus appears to be insignificant even in the extreme case of a thermally driven boundary layer, but the argument is perhaps not conclusive, and the contribution of thermal scattering is included in §§6–8. In any event, inertial scattering is never unimportant compared with thermal scattering.

3. Solution of the scattering equation

The formal solution of (2.2) is easy to write down, but it needs considerable reduction before the essential physics of scattering emerges. The reduction depends upon the fact that sound scattered to a point behind a shock at a given time has a two-dimensional domain of dependence. The geometry of that surface of dependence is fundamental to the problem of shock-wave scattering.

Figure 5 shows the shock SS' at some time t greater than zero, after it has passed through the observation point O . The shock is currently located a distance

$$h = c_0 t$$

along the x -axis behind the observation point. The appearance of the delta function in (2.2) implies that scattered waves are excited by intense interactions concentrated entirely in the plane of the shock: only as the shock front passes through it does an eddy emit a secondary wave. When, at some time in the past, the shock passed the eddy (or thermal inhomogeneity) at point P , the interaction between the two resulted in the emission of a secondary wave, which since then has been propagating outward from its point of origin P . Now suppose that the eddy at P happens to be one of those responsible for the perturbation received by O at time t . Since the shock and the scattered wave both travel at the ambient speed of sound c_0 under the present approximations, the distance PO from the scattering centre to the observation point must equal the perpendicular distance PS from the scattering centre to the shock. Only points P satisfying the condition $PO = PS$ contribute to the perturbation received at time t . The locus of

those points is a paraboloid whose focus is the observation point and whose directrix is the shock. That surface is called here the paraboloid of dependence. The vertex V of the paraboloid lies half-way between the observation point and the shock, and the radius of curvature of the paraboloid at its vertex is $\frac{1}{2}h$. The

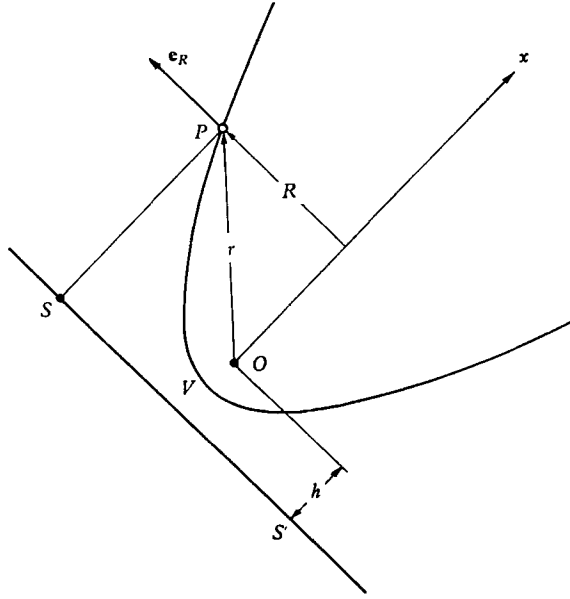


FIGURE 5. Geometry of the paraboloid of dependence. O is the observation point, P is a scattering centre, V is the vertex of the paraboloid, and SS' is the shock, which is propagating downward and to the left.

axis of the paraboloid of dependence coincides with the co-ordinate x introduced already, and the radius R of the paraboloid satisfies the equation

$$R = [2h(x + \frac{1}{2}h)]^{\frac{1}{2}}. \quad (3.1)$$

Distances h of interest are 50 ft. and less, very much smaller than the thickness of the boundary layer where the scattering takes place. On the scale of the boundary-layer thickness, the paraboloid appears as a slender column, a wake of dependence so to speak, extending behind the shock (figure 6). The approximation

$$R \approx (2hx)^{\frac{1}{2}} \quad (3.2)$$

is valid almost everywhere on the paraboloid for all reasonable values of h . R is typically 200 ft. in a boundary layer 2000 ft. thick. The slenderness of the paraboloid of dependence determines many of the qualitative attributes of N -wave distortions and leads to important analytical simplifications later on.

Because the fluid is being regarded as unbounded for the time being, the formal retarded-potential solution of (2.2) is a volume integral taken over all space (Phillips 1933). Suppose that r is the distance from the observation point to a volume element dV . Then the integrand is minus the right-hand side of (2.2), evaluated at the retarded time $(t - r/c_0)$ and weighted by the factor $(4\pi r)^{-1}$. On the basis of the foregoing discussion, it is natural to try to transform the volume

integral into a surface integral over the paraboloid of dependence. The choice of cylindrical co-ordinates (x, R, ϕ) as the variables of integration facilitates the transformation. The volume element dV is then $R dx dR d\phi$, and the expression for the fractional pressure perturbation $s(0, t)$ is as follows:

$$s(0, t) = -\frac{1}{4\pi} \int_{-\infty}^{\infty} dx \int_0^{\infty} dR \int_0^{2\pi} R d\phi \left(\frac{\partial}{\partial x} \left\{ \frac{2m(x, R, \phi, t - r/c_0) \delta(x + h - r)}{r} \right\} \right)_{R, r}. \quad (3.3)$$

R is used here as the radial co-ordinate of a general point in space, not necessarily lying on the paraboloid of dependence, and ϕ is the angular co-ordinate measured from the x_2 -axis. The distance r is a function of x and R ,

$$r = (x^2 + R^2)^{\frac{1}{2}}, \quad (3.4)$$

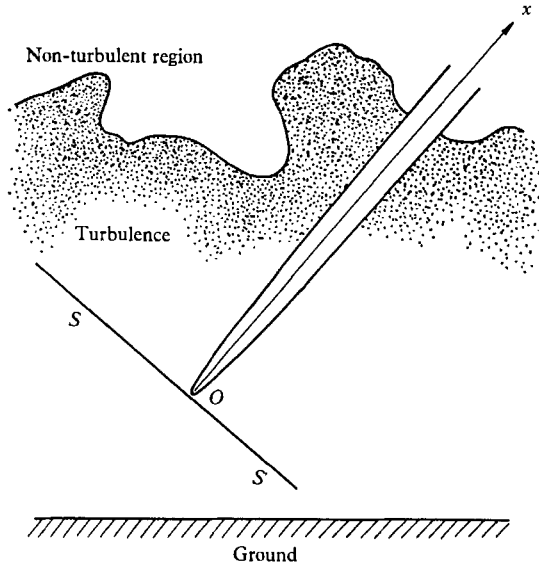


FIGURE 6. Paraboloid of dependence viewed from a distance comparable to the height of the turbulent boundary layer.

but, as the subscripts R, r on the derivative under the integral suggest, not only R but also r is held fixed during the differentiation of the quantity in curly brackets. That is why r could be brought inside the brackets. Note that it is the derivative on the right-hand side of (2.2) that is being evaluated at the retarded time, rather than the quantity $\{2m(\mathbf{x}, t) \delta(x + c_0 t)\}$ itself.

The quantity inside the curly brackets in (3.3) has the form $f(x, R, r)$, the dependence on ϕ and t being understood, and any such function satisfies the following identity for the $r(x, R)$ of (3.4):

$$\left(\frac{\partial f}{\partial x} \right)_R = \left(\frac{\partial f}{\partial x} \right)_{R, r} + \frac{x}{R} \left[\left(\frac{\partial f}{\partial R} \right)_x - \left(\frac{\partial f}{\partial R} \right)_{x, r} \right]. \quad (3.5)$$

The left-hand side of (3.5) is the total derivative of f with respect to its dependence both on x and r , r being allowed to vary according to (3.4). The first term on the right is the derivative of f with respect to its explicit dependence on x only. The quantity in square brackets is the rate of change of f with respect to R due solely

to f 's dependence on r . The factor x/R converts the term into the rate of change of f with respect to x due solely to f 's dependence on r . The identity (3.5) permits (3.3) to be written in the following form:

$$s(0, t) = -\frac{1}{2\pi} \int_{-\infty}^{\infty} dx \int_0^{\infty} dR \int_0^{2\pi} d\phi \left[\left(\frac{\partial}{\partial x} \left(\frac{R}{r} m \delta(x+h-r) \right) \right)_R - \left(\frac{\partial}{\partial R} \left(\frac{x}{r} m \delta(x+h-r) \right) \right)_x + \frac{x}{r} \left(\frac{\partial m}{\partial R} \right)_{x,r} \delta(x+h-r) \right], \quad (3.6)$$

where the argument of m is $(x, R, \phi, t-r/c_0)$ as in (3.3).

The argument $(x+h-r)$ of the delta functions is negative everywhere if h is negative. It follows from (3.6) that $s(0, t) = 0$ for $t < 0$, in other words, that no scattered waves reach the observation point ahead of the shock. The task remains to simplify (3.6) for $h \geq 0$. That task is accomplished in the following discussion, which involves some manipulations with delta functions. All the manipulations can be justified rigorously by treating a shock of finite thickness and allowing the thickness to approach zero after the integrals have been evaluated. A thin ramp shock proves particularly suitable; the delta functions in (3.6) give way to narrow top-hat functions. In the discussion, the symbols (I), (II), and (III) denote the integrals of the first, second, and third terms in the integrand of (3.6).

The first term in the integrand is an ordinary partial derivative and can be integrated immediately over x for fixed R, ϕ . The result is zero, since m is zero for large enough x and $\delta(x+h-r)$ is zero for all $x < -\frac{1}{2}h$:

$$(I) = 0.$$

The fact that (I) is zero for h identically equal to zero is one of the points that can be checked by means of a shock of finite thickness.

The second term in the integrand of (3.6) is also a partial derivative and can be integrated over R for fixed x, ϕ and then integrated again over ϕ :

$$\begin{aligned} (II) &= -\frac{1}{2\pi} \int_{-\infty}^{\infty} dx \int_0^{2\pi} d\phi \operatorname{sgn}(x) m(x, 0, \phi, t-|x|/c_0) \delta(x+h-|x|), \\ &= -\int_{-\infty}^{\infty} dx \operatorname{sgn}(x) m_A(x, t-|x|/c_0) \delta(x+h-|x|), \end{aligned}$$

where the subscript A denotes conditions on the x -axis. The final integration over x yields $\frac{1}{2}m_V(t-h/2c_0)$ for $h > 0$, where V denotes conditions at the vertex of the paraboloid of dependence. At $h = 0$, however, the argument of the delta function in the second expression for (II) is zero for all positive x , and the integral is infinite. The infinity is, in fact, a delta-function singularity concentrated at $h = 0$.† The weight of the singularity can be found by integrating (II) over h in a small interval around $h = 0$, with the result that

$$(II) = -\delta(h) \int_0^{\infty} m_A(x, t-x/c_0) dx + \frac{1}{2}m_V(t-h/2c_0).$$

† I am grateful to J. E. Ffowcs Williams of Imperial College for pointing out the singularity. It was omitted in the earlier version of this paper (Crow 1968), and consequently there appeared to be a gulf between the present theory and that of Lighthill (1953). The singularity brings the theories closer together and, moreover, admits a simple physical interpretation as a phase shift.

The third term in the integrand of (3.6) can also be integrated over R . The delta function singles out values of the quantity $(x/r) (\partial m/\partial R)_{x,r}$ on the surface defined by the condition $r = x + h$, which is an alternative form of the equation (3.1) for the paraboloid of dependence. The variation of $(x + h - r)$ with respect to R weights the contribution from each point on the paraboloid by the factor

$$(\partial r/\partial R)_x^{-1} = r/R, \tag{3.7}$$

so the result of the integration is that

$$(III) = -\frac{1}{2\pi} \int_{-\frac{1}{2}h}^{\infty} dx \int_0^{2\pi} d\phi \left\{ \frac{x}{R} \left(\frac{\partial m}{\partial R} \right)_{x,r} \right\}_P,$$

where the subscript P means that the quantities are to be evaluated on the paraboloid of dependence.

The fractional perturbation $s(0, t)$ is the sum (I) + (II) + (III). It is convenient to indicate that a quantity is to be evaluated at an appropriately retarded time by putting square brackets around it. The quantity $m_V(t - h/2c_0)$ appearing in the expression for (II), for example, can be written as $[m]_V$, which means the value that m took at the vertex of the current paraboloid at the earlier time $(t - h/2c_0)$ when the shock passed that point. $(\partial m/\partial R)_{x,r}$ in (III) is likewise the radial component of the gradient of m , evaluated at point P at the time $(t - r/c_0)$ when the shock passed P . $(\partial m/\partial R)_{x,r}$ can therefore be written as $[\mathbf{e}_R \cdot \nabla m]_P$, where \mathbf{e}_R is the radial unit vector shown in figure 5. In terms of the square-bracket notation,

$$s(0, t) = -\delta(h) \int_0^{\infty} [m]_A dx + \frac{1}{2} [m]_V - \frac{1}{2\pi} \int_{-\frac{1}{2}h}^{\infty} dx \int_0^{2\pi} d\phi \frac{x}{R} [\mathbf{e}_R \cdot \nabla m]_P. \tag{3.8}$$

A more suggestive expression for $s(0, t)$ is obtained by writing $\delta(h)$ as a derivative of the Heaviside function ($\delta(h) = dH(h)/dh = c_0^{-1}dH(t)/dt$) and by transforming the double integral in (3.8) into a surface integral over the paraboloid of dependence. Thus

$$s(0, t) = \tau dH(t)/dt + \psi(t), \tag{3.9}$$

where
$$\tau = c_0^{-2} \int_0^{\infty} [c_\theta - u_1]_A dx, \tag{3.10}$$

and
$$\psi(t) = \begin{cases} \frac{1}{2} [m]_V - \frac{1}{2\pi} \iint_{\text{parab.}} dA \frac{x}{R(2rh)^{\frac{1}{2}}} [\mathbf{e}_R \cdot \nabla m]_P & \text{for } t \geq 0, \\ 0 & \text{for } t < 0. \end{cases} \tag{3.11}$$

The quantities R and r appearing in (3.8) and (3.11) now are associated with points on the paraboloid of dependence. They satisfy (3.1) and (3.4) and are shown in figure 5. As usual, $h = c_0 t$.

The first term on the right of (3.9) is written as a derivative of the Heaviside function to emphasize its role as a phase shift. Equation (3.9) represents a perturbation on the zeroth-order shock, which travels at the ambient speed of sound c_0 and arrives at the observation point at time 0. The real shock travels at the slightly different speed $(c_0 + c_\theta - u_1)$ and, to first-order in u_1/c_0 and c_θ/c_0 , reaches the observation point at minus the time τ given in (3.10). First-order scattering theory

represents the change as the derivative of the wave-form history times the phase shift. Since the shock has been idealized as a discontinuity, the resulting term in (3.9) is singular.

Phase shifts are not measured in sonic-bang experiments and have nothing to do with the kind of wave-form distortions shown in figure 3. The function $\psi(t)$ defined by (3.11) represents the observable distortions. The first term on the right of (3.11) represents a purely local effect, an extra compression caused by the flow of air into the shock, for example, if u_1 dominates c_θ . That term is always very small. The second term represents a sum of contributions that arise everywhere the paraboloid of dependence intercepts an eddy or a temperature inhomogeneity. The second term therefore must contain the explanation of the spiky fine structure of N -waves. It is interesting that only the radial component of ∇m contributes to extensive scattering. Inertial scattering, according to the definition of m under (2.2), involves only the component u_1 of eddy velocity normal to the shock. According to (3.11), moreover, only derivatives of that component parallel to the plane of the shock scatter extensively.

Imagine now a succession of weak shocks passing the observation point. Each shock scatters independently, to the extent that non-linear steepening and second scattering are negligible, and each set of scattered waves satisfies an equation of the form (3.9) with a suitable time delay. A plane wave of arbitrary form can be synthesized out of infinitesimal pressure jumps, and the corresponding scattered field can be found by summing contributions like (3.9). There results a general solution of the first-order scattering problem for plane waves:

$$p(t) - p_0 = p^N(t) + \tau \frac{dp^N(t)}{dt} + \int_{-\infty}^{\infty} \psi(t-t') \frac{dp^N(t')}{dt'} dt'. \quad (3.12)$$

$p^N(t)$ is the pressure history that would have been observed, had there been no scattering. The function $\psi(t-t')$, obtained originally as the response of the scattering field $m(\mathbf{x})$ to a unit step function (the shock), appears in (3.12) as the kernel in a Duhamel's-integral solution of the general problem. Since the detailed state of the atmosphere changes with time, ψ and τ are implicit functions of t . The atmospheric changes are slight during the passage time of an N -wave, however, so the dependence on t can be ignored for practical purposes. Equation (3.12) confirms, for continuous $p^N(t)$, the interpretation of τ as a phase shift: the first two terms on the right-hand side are the leading terms of the Taylor series for the time-shifted but otherwise undistorted wave-form $p^N(t+\tau)$. They could reasonably be written as $p^N(t+\tau)$, in fact, but the Taylor-series form is retained for the purpose of comparison with certain aspects of Lighthill's treatment of scattering.

4. Infinite forward scattering, and ray acoustics

Acoustic scattering theory, as formulated by Lighthill (1953), predicts an infinite rate of scattering toward a shock. In order to understand infinite forward scattering in the light of (3.12), let us forget for a moment that the term $\tau dp^N/dt$ results from a phase shift and imagine that it represents a scattered wave some-

how distinct from the incident wave. The term can be very large for rapidly varying $p^N(t)$, numerically much larger than the integral in (3.12) representing actual wave-form distortions. For a thin shock, $\tau dp^N/dt$ might be interpreted as an intense pulse dominating all other scattered waves. According to that interpretation, the total energy scattered into the field per unit area of shock has an average value

$$E^S = \frac{1}{\rho_0 c_0^2} \int_{-\infty}^{\infty} \langle (p^S)^2 \rangle dx = \frac{\langle \tau^2 \rangle}{\rho_0 c_0} \int_{-\infty}^{\infty} \left(\frac{dp^N}{dt} \right)^2 dt,$$

where angle brackets denote ensemble averages. $\langle \tau^2 \rangle$ is the mean-square phase shift at the shock front. If thermal scattering is neglected,

$$\langle \tau^2 \rangle = \frac{1}{c_0^4} \int_0^{\infty} dx \int_0^{\infty} dx' \langle [u_1]_A [u_1]_{A'} \rangle = 2LX \frac{\langle u_1^2 \rangle}{c_0^4},$$

where L is the integral scale of the turbulence (cf. Lighthill 1953, p. 538) and X is the distance along the ray axis from the shock front to the boundary of the turbulent region. Assumptions have been made in accord with Lighthill's treatment that the turbulence is homogeneous and that $X \gg L$, although neither assumption applies to atmospheric turbulence. Since equal volumes of turbulence behind the shock contribute equally to E^S under the assumption of homogeneity, the mean energy e^S scattered from a unit volume of turbulence as the shock passes through is E^S/X . As a result of combining the expressions for E^S and $\langle \tau^2 \rangle$,

$$e^S = \frac{2L \langle u_1^2 \rangle}{\rho_0 c_0^5} \int_{-\infty}^{\infty} \left(\frac{dp^N}{dt} \right)^2 dt, \quad (4.1)$$

which has the same meaning as Lighthill's equation (57). As the incident wave $p^N(t)$ steepens toward the limit of a discontinuous shock, e^S diverges toward infinity. Lighthill concludes that a shock produces an infinite amount of scattered energy and removes the divergence by introducing non-linear effects extraneous to first-order scattering theory: most of the waves are supposed to catch up with the shock and recombine with it.

It is clear from the foregoing derivation of (4.1), however, that the apparent energy divergence is due entirely to the phase shift, which scattering theory is bound to represent in series form. The scattered energy given in (4.1) is not carried by wave-form distortions and would not be noticed by an observer unaware of detailed phase relationships. Put another way, the scattered energy in (4.1) is compensated by an energy loss in the so-called incident wave (as Lighthill shows for sinusoidal waves in the appendix to his paper). An essential advantage of presenting the solution of the scattering equation in the form (3.12) is that genuine wave-form distortions can be distinguished from the phase shift. From the present viewpoint, it would be unnatural to treat the phase shift as an infinitely energetic acoustic pulse requiring a special mechanism for its removal.

The function $\psi(t)$, which represents observable shock distortions, is finite at time zero when the shock and the observation point coincide, and it remains finite thereafter. It is obvious from (3.11) that ψ is finite after the shock passes, because $h > 0$ if $t > 0$, and the R^{-1} singularity at the vertex of the paraboloid is integrable. The fact that ψ approaches a finite limit $\psi(0)$ as t and h approach zero through

positive values is not so obvious and requires proof. In this instance it is easier to use the double integral in (3.8) rather than the equivalent surface integral in (3.11). The paraboloid of dependence closes down on the x -axis as $h \rightarrow 0$, and $R(x, h) \rightarrow 0$ throughout the scattering region. As R decreases everywhere below the scale of the finest eddies,

$$\frac{1}{\pi R^2} \int_0^{2\pi} R[\mathbf{e}_R \cdot \nabla m]_P d\phi \rightarrow [\nabla_1^2 m]_A$$

by the divergence theorem. $\nabla_1^2 m$ is the two-dimensional Laplacian of m , involving only the two derivatives parallel to the shock; in the Cartesian co-ordinates of § 2, $\nabla_1^2 = \partial^2/\partial x_2^2 + \partial^2/\partial x_3^2$. The subscript A refers as usual to conditions on the x -axis. $\psi(t)$ thus tends to a finite limit $\psi(0)$, the fractional pressure perturbation at the shock:

$$\psi(0) = \frac{1}{2} \left(m_O - \int_0^\infty x[\nabla_1^2 m]_A dx \right), \quad (4.2)$$

where the subscript O denotes conditions at the observation point.

Equation (4.2) is valid only for small perturbations $\psi(0)$. The amplitude of an ideally discontinuous and infinitesimal shock can be computed exactly by the method of ray acoustics, which is a special case of a general theory of the propagation of discontinuities in hyperbolic systems (Courant & Hilbert 1965, chapter VI, § 4). Strong amplifications $\{1 + \psi(0)\}$ must be determined by numerical integration along ray tubes (Friedman *et al.* 1963), but ray acoustics can be linearized for small $\psi(0)$ to yield a closed-form solution analogous to (4.2):

$$1 + \psi(0) = \exp \left\{ \frac{1}{2} \left(m_O - \int_0^\infty x[\nabla_1^2 m]_A dx \right) \right\} \quad (4.3)$$

(cf. Chernov 1960; the local contribution m_O is usually omitted). The quantity m in (4.3) is being interpreted here according to (2.3) as the departure of the generalized index of refraction from unity. Fluctuations in the index of refraction focus and defocus the advancing shock front, and the integral shared by (4.2) and (4.3) represents the accumulated amplification of the pressure jump across the shock. The same phenomenon causes stars to twinkle, although the acoustic and electromagnetic indices of refraction are of course quite different.

To the extent that $\psi(0)$ is small, equations (4.2) and (4.3) are essentially the same, and scattering theory includes ray acoustics as a limiting case. If the perturbations are large, however, then second scattering is important, and the assumptions underlying (3.11) and its limit (4.2) break down. Equation (4.2) suggests the obviously unphysical result, for example, that the pressure jump $\Delta p\{1 + \psi(0)\}$ can be negative if the shock is highly defocused. Linearized ray acoustics also breaks down, one consequence being that (4.3) does not admit the possibility of the shock coming to a concentrated focus ($\psi(0) \rightarrow \infty$) at a finite distance inside the turbulent region. The fully non-linear theory of ray acoustics remains valid for strong amplifications of an infinitesimal shock, but it gives no information analogous to (3.11) about the pressure field behind the shock. Any wave-form varying rapidly enough to satisfy the conditions of ray acoustics is

merely focused or defocused uniformly by the factor $\{1 + \psi(0)\}$. Ray acoustics clearly cannot explain the fine structure of N -waves; the limitations of scattering theory must be tolerated.

The relation between non-linear ray acoustics and first-order scattering theory, in the context of the shock-wave problem, can be summarized as follows. *Scattering theory is valid for arbitrary radii of the paraboloid of dependence but is restricted to small perturbations ψ . Ray acoustics is valid for arbitrary ψ but applies only if the radius of the paraboloid of dependence is everywhere much smaller than the finest inhomogeneities in the medium.* In the case of a periodic incident wave, the wavelength determines whether ray acoustics is applicable. An idealized pressure jump has no length scale of its own, and the size of the paraboloid of dependence provides the criterion.

5. Qualitative implications of scattering theory

Even without further analysis, the predictions of scattering theory can be checked against the experimental observations listed in §1. The perturbations behind the N -wave shocks are treated from here on as though they were scattered from isolated shocks; scattering from the expansion wave between the shocks is neglected. The general solution (3.12) can be used to validate that approximation for times after the passage of a shock that are short compared with the duration of the N -wave. The phase shift in the solution (3.9) of the shock-wave problem has no bearing on spiky distortions and does not enter the discussion of §§5–8. Explanations of the five attributes listed in §1 must rest on the function $\psi(t)$ and, more specifically, on the integral in (3.11) over the paraboloid of dependence. The fact that those attributes depend mainly on the *geometry* of the paraboloid of dependence is strong evidence that scattering is the real source of sonic-bang distortions. The following explanations are numbered to match the attributes in §1:

(1) The perturbations are random because the mean temperature and velocity fields merely focus or defocus the incident N -wave slightly. Scattering theory has been discussed so far in terms of ‘eddies’ and ‘temperature inhomogeneities’, but the quantity ∇m appearing in (3.11) may contain mean velocity and temperature gradients as well. It is apparent from figure 6, however, that the radius R of the paraboloid of dependence is much smaller than the mean-field scale, the height δ of the boundary layer say, for any reasonable distance h between the shock and the observation point. As far as the mean field is concerned, the approximation (4.2) applies to all $\psi(t)$, and the mean field focuses or defocuses the N -wave uniformly. Figure 7 shows how the expansion between the shocks rocks under the action of a mean field. The rocking certainly has nothing to do with the spiky structure, and, besides, it is a very small effect. If $\langle m \rangle$ is a typical Mach number or dimensionless temperature variation of the mean field, then the integral in (4.2) is of order $\delta^2 \langle \langle m \rangle / \delta^2 \rangle \sim \langle m \rangle$, the same order as the local contribution. Rocking is thus an $O(\langle m \rangle)$ effect. $\langle m \rangle$ may be ten times larger than a typical turbulent Mach number, but it will not be greater than 0.1 in the vicinity of an

intelligently flown aircraft. The effect of the mean field is therefore negligible. From now on, $m(\mathbf{x}, t)$ is treated as a random field with zero mean.

(2) The perturbations are large because, roughly speaking, a great many individually weak interactions contribute to the scattered wave. Interactions represented by the quantity $[\mathbf{e}_R \cdot \nabla m]_P$ are integrated over the whole surface of the paraboloid of dependence. Individual interactions are $O(m)$, but their sum is large. That does not explain why the perturbations tend to decrease with time after the passage of the shock. Since the paraboloid opens out and acquires more area as h increases, it might seem that the perturbations would increase. The reason they do not is that the interaction $[\mathbf{e}_R \cdot \nabla m]_P$ is weighted with the factor x/R , which approaches infinity as $h \rightarrow 0$. The factor x/R came in through (3.7) and represents the effectiveness of scattering almost directly forward.

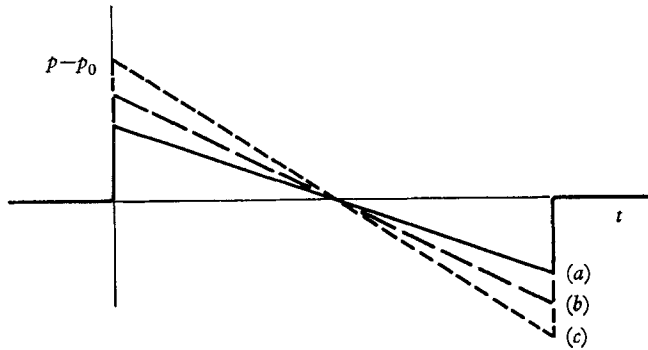


FIGURE 7. Rocking of an N -wave in a large-scale mean field: (a) defocused; (b) normal; (c) focused.

(3) The length scale of the perturbations is short because the paraboloid of dependence filters out contributions from eddies much larger than its local radius $R(x, h)$. As the integral in (3.11) is carried around a perimeter at a fixed station x , the vector \mathbf{e}_R rotates full circle, the part of ∇m arising from large eddies remains nearly constant, so the corresponding contributions to $[\mathbf{e}_R \cdot \nabla m]_P$ cancel during the integration. Contributions from very small eddies tend to cancel at random. The net result is that eddies of scale $R(x, h)$ are mainly responsible for the wave that scatters from x and arrives at the observation point at time h/c_0 . The argument fails if no eddies of that scale exist, but the turbulent energy cascade assures a rich supply (that statement is made quantitative in § 7). The scale $R(x, h)$ does not directly characterize the N -wave perturbations, since only a small change in h is needed to bring about a considerable change in R over most of the paraboloid. If h changes by an amount comparable to itself, then R also changes by an amount comparable to itself according to (3.2), and the paraboloid expands enough to intercept a new set of scattering eddies. The pressure perturbation at the observation point must undergo a considerable change as well. The typical length λ of the perturbations is therefore comparable to h : $\lambda(h) \sim h$. The spike length $\lambda(h)$ is much smaller than the typical scale, $R(\delta, h)$ say, of the scattering eddies and very much smaller indeed than the integral scale of the turbulence

(cf. § 6). Moreover, $\lambda(h)$ grows with h , in conformity with the experimental evidence (figure 3). The fine structure of an N -wave is a filtered and high compressed image of the turbulence that the wave has encountered.

(4) The leading and trailing shocks share a common fine structure because the scattered waves that arrive at a fixed observation point at a given time after the passage of the trailing shock come from the same paraboloid of dependence as those waves that arrived a similar time after the passage of the leading shock. The coincident paraboloids are separated in time, of course, by the 200 ms passage time of the N -wave. They intercept slightly different eddy patterns in spite of their geometrical similarity, but 200 ms is not enough time for the wind to carry eddies a significant distance through the surface of a given paraboloid. That is the sense in which the turbulence is frozen.

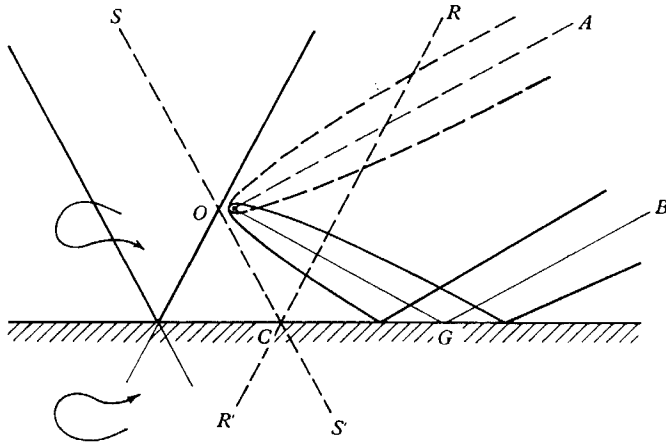


FIGURE 8. Reflexion of a paraboloid of dependence from the ground. The solid and dashed lines refer to separate instants of time, the solid line corresponding to the later instant.

(5) The phenomenon shown in figure 4 depends on the reflexion of incident and scattered waves from the ground. The analysis has been carried out so far without regard for the ground, as though the fluid were unbounded. If the ground is flat, as assumed here, then the method of images can be used to extend all the results obtained so far to account for reflexion. The procedure is illustrated in figure 8, where the oblique lines correspond to, say, the leading shock of the N -wave. The observation point O is located on a tower some distance above the ground. If there were no ground, then the incident shock front would be an infinite plane SS' , and there would be a uniform downward component of velocity behind the shock. The downward component of velocity, which must in fact be zero at ground level, can be eliminated without introducing the ground explicitly by assuming that a second shock RR' propagates upward in the hypothetical unbounded medium. The resulting shock-wave flow satisfies the boundary condition at the ground. The flow above ground level is the same as that realized in actuality, and the flow below ground level is its image. SC is the incident shock, CR is the reflected shock, and $R'CS'$ is the hypothetical image flow. The eddies

can be reflected through the ground in the same way, as shown at the left in figure 8. Thus the whole system of shocks and eddies above the ground can be treated as part of a combined system of real and image flows in an unbounded medium. The paraboloid of dependence for waves scattered by the incident shock SC to the observation point O extends upward along the axis OA . Now consider the shock system at a later time when the reflected shock is as far behind O as SC was; the shock system at that later time is shown by the oblique solid lines in the figure. The paraboloid of dependence for the reflected shock extends downward from O to the ground at G and there passes into the image flow underneath. Equivalently, the paraboloid can be regarded as having been reflected upward from G along the axis GB . *The paraboloid of dependence reflects from the ground just as the shock does.* Waves scattered to O by the reflected shock emanate from the reflected paraboloid OGB . Even though the reflected shock is exactly as far behind the observation point as the incident shock was at the earlier time, the corresponding paraboloids do not coincide. Instead they follow widely separate paths OA and OGB , and they intercept entirely different eddies. That is why a microphone on a tower records different spikes behind incident and reflected shocks. The difference has little to do with the passage of the reflected wave through an extra layer of eddies between the microphone and the ground. The fact that scattering theory accounts so simply for the peculiar phenomenon shown in figure 4 is perhaps the strongest qualitative argument in its favour.

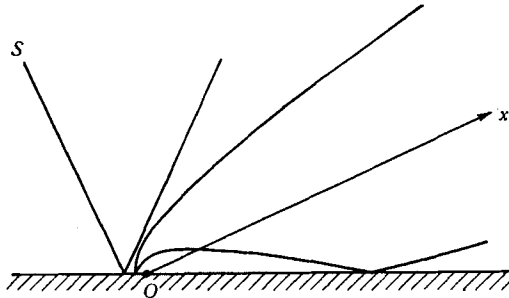


FIGURE 9. Surface of dependence for an observation point on the ground.

In the statistical analysis that follows, the observation point is assumed to be situated on the ground. The paraboloids of dependence associated with the incident and reflected waves then coincide. The ratio of the scattered pressure p^S to the pressure jump across the incident shock alone is twice the right-hand side of (3.8), where the integral is carried over the indented paraboloid shown in figure 9. Reflexion also doubles the basic pressure jump, however, so (3.8) and (3.9) are valid as they stand if $s(0, t)$ is understood to be the perturbation at the ground divided by the net unperturbed pressure jump at the ground. The only change is that the integrals in (3.8) and (3.11) must be carried over the little cap above the observation point (figure 9) wherever the original paraboloid lies below ground level; the vector \mathbf{e}_R on the cap points upward and to the right, parallel to the reflected shock. The contribution from the cap is negligible, and the slight indentation on the paraboloid of dependence is not discussed further.

6. Mean-square pressure perturbation

Scattering theory appears to explain the qualitative features of N -wave perturbations, but it remains to show that $\psi(t)$ compares quantitatively with the fractional pressure perturbations observed in experiments. Since $\psi(t)$ is random, some statistical property is required, and the easiest one to predict analytically is $\langle \psi^2(t) \rangle$. The angle brackets denote an average over an ensemble of pressure histories recorded under identical flight and meteorological conditions. $\psi(t)$ comprises the second and third terms on the right of (3.8), but only the third which represents extensive scattering is significant. Thus

$$\langle \psi^2(t) \rangle = \frac{1}{(2\pi)^2} \int_{-\frac{1}{2}h}^{\infty} dx \int_{-\frac{1}{2}h}^{\infty} dx' \int_0^{2\pi} d\phi \int_0^{2\pi} d\phi' \left(\frac{xx'}{RR'} \right) \langle [\mathbf{e}_R \cdot \nabla m]_P [\mathbf{e}_R \cdot \nabla m]_{P'} \rangle. \quad (6.1)$$

In order to perform the integration, one would hold point P fixed and allow P' to range over the surface of the paraboloid of dependence as shown in figure 10. The procedure can be repeated for each P and the results summed. The heavy arrows in figure 10 represent the directions of the gradients of m relevant at points P and P' . The vector distance from P to P' is σ , whose scalar magnitude is denoted by σ in the following discussion.

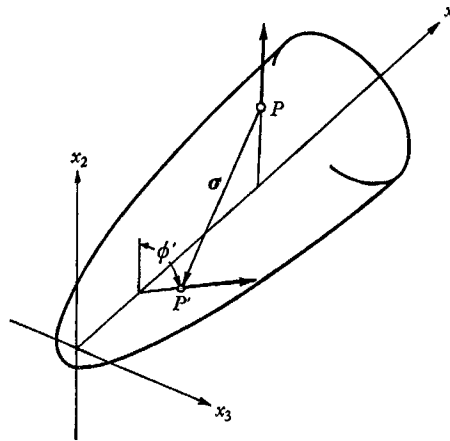


FIGURE 10. Geometry of the double integration over the paraboloid of dependence.

Figure 11 gives an indication of the size of the energy-bearing eddies that the paraboloid of dependence intercepts on its way up through the turbulent boundary layer. The co-ordinate y is the altitude, and the distance between the dotted lines is $L(y)$, a rough compromise between the vertical and horizontal integral scales of the turbulence. L grows linearly with y in the first several hundred feet of the boundary layer and rapidly outstrips the parabolically growing radius R of the paraboloid of dependence. In the upper part of the layer, $L(y)$ levels off at a significant fraction of the total boundary-layer thickness δ , which may be 3000 ft. R is nowhere greater than about 300 ft. for significant values of h , so the paraboloid is slender compared not only with its own length, $R \ll x$, but also with the local integral scale of the turbulence, $R \ll L$. The inequalities

$R \ll x$ and $R \ll L$ apply everywhere save near the vertex of the paraboloid, and scattering from that small part of the surface is negligible anyway.

The correlation $\langle m_P m_{P'} \rangle$ between values of m drops to zero only as σ substantially exceeds the local integral scale L . The scattering correlation $\langle [\mathbf{e}_R \cdot \nabla m]_P [\mathbf{e}_R \cdot \nabla m]_{P'} \rangle$ contains *gradients* of m , however, so the scale relevant to scattering need not be L . The argument in § 5 concerning attribute (3) suggests that R rather than L is the scale of the eddies that contribute most to scattering. That argument is confirmed in § 7, where the integral over P' in (6.1) is shown to converge for separations σ comparable to R , under quite realistic assumptions

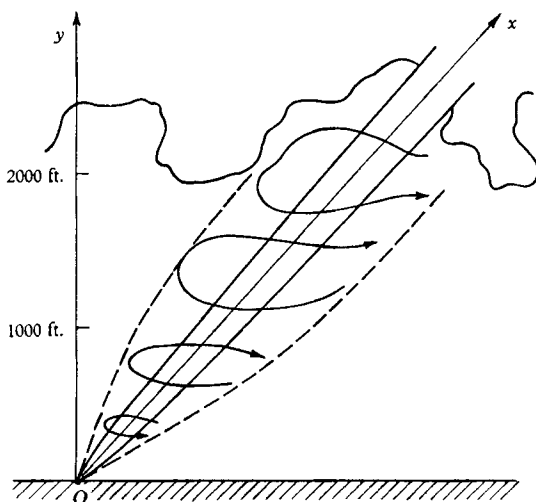


FIGURE 11. Relation between the size of the energy-bearing eddies and the radius of the paraboloid of dependence.

about atmospheric turbulence. Convergence for $\sigma \sim R$, combined with the inequalities $R \ll x$ and $R \ll L$, permits several simplifications of (6.1), without which the integral could not be evaluated analytically:

(i) The retarded times at P and P' differ by a negligible interval of order R/c_0 , so the scattering correlation in (6.1) can be replaced with the correlation $\langle (\mathbf{e}_R \cdot \nabla m)_P (\mathbf{e}_R \cdot \nabla m)_{P'} \rangle$ involving a spatial separation only.

(ii) Wherever the scattering correlation is significant, the geometrical factor (xx'/RR') can be replaced with (x^2/R^2) .

(iii) Eddies on the scale $R \ll L$ are practically isotropic, since whatever anisotropy is present at the large scale L is lost in the cascade down to scales comparable to R . The scattering correlation $\langle (\mathbf{e}_R \cdot \nabla m)_P (\mathbf{e}_R \cdot \nabla m)_{P'} \rangle$ depends only on the difference between ϕ and ϕ' , as a consequence, not on ϕ and ϕ' separately. The integration over ϕ' can be carried out for the particular P shown in figure 10, chosen so that $(\mathbf{e}_R)_P$ is aligned with the x_2 -axis. The remaining angular integration over ϕ can be replaced with the factor 2π .

(iv) At almost all stations x , the radius $(2hx)^{\frac{1}{2}}$ of the paraboloid at P is practically the same as its radius $(2hx')^{\frac{1}{2}}$ at P' for the separations σ comparable to R . P' can therefore be regarded as lying on a cylindrical sleeve fitted to the paraboloid at x . The construction is shown in figure 12. The vector σ can be written in component form as (ξ, η, ζ) in the co-ordinates shown. The axes (ξ, η, ζ) are parallel to the original axes (x, x_2, x_3) .

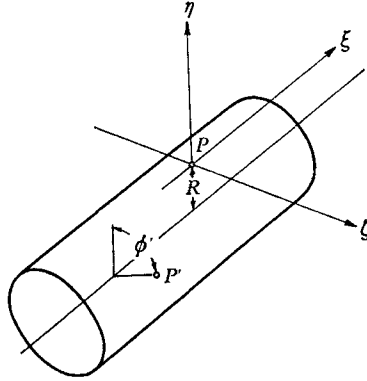


FIGURE 12. Geometry of the cylindrical sleeve fitted locally to the paraboloid of dependence.

Equation (6.1) simplifies considerably as a result of these first four approximations:

$$\langle \psi^2(t) \rangle = \frac{1}{2\pi} \int_0^\infty dx (x^2/R^3) \iint_{\text{cyl.}} dA \langle (\mathbf{e}_R \cdot \nabla m)_P (\mathbf{e}_R \cdot \nabla m)_{P'} \rangle, \quad (6.2)$$

where $R = (2hx)^{\frac{1}{2}}$ and $h = c_0 t$. The surface integration extends over the cylindrical sleeve, of radius R , fitted locally to the original paraboloid of dependence. Since $(\mathbf{e}_R)_P$ is aligned with the x_2 -axis, the scattering correlation in (6.2) can be expanded in terms of Cartesian derivatives of m as follows:

$$\langle (\mathbf{e}_R \cdot \nabla m)_P (\mathbf{e}_R \cdot \nabla m)_{P'} \rangle = \left\langle \left(\frac{\partial m}{\partial x_2} \right)_P \left(\frac{\partial m}{\partial x_2} \right)_{P'} \right\rangle \cos \phi' + \left\langle \left(\frac{\partial m}{\partial x_2} \right)_P \left(\frac{\partial m}{\partial x_3} \right)_{P'} \right\rangle \sin \phi'. \quad (6.3)$$

Two additional properties of fine-scale turbulence lead to a further reduction of the expression for $\langle \psi^2(t) \rangle$:

(v) The turbulence is homogeneous over distances of order R . The statistical structure of eddies of size R varies significantly over distances comparable to L , but not over distances comparable to R . Let us define the structure function D of the scattering field m as follows:

$$D(\boldsymbol{\sigma}, x) = \langle \{m_{P'} - m_P\}^2 \rangle.$$

The co-ordinate x uniquely specifies the location of P on the surface of the paraboloid of dependence (cf. figure 10), and $\boldsymbol{\sigma}$ then specifies the location of P' . The structure function is zero for $\boldsymbol{\sigma} = 0$, and for the sake of the present argument it

can be regarded as having the form $f(x)\sigma^n$ for $\sigma \sim R$, where $f(x)$ varies over distances $\sim L$ and where $n \sim 1$ (cf. equations (7.1)). Then $\partial D/\partial x \sim (R/L)\partial D/\partial \xi$, for example, so derivatives of D with respect to x are negligible for the separations σ of interest. After a little manipulation, it follows from (6.3) that

$$\langle (\mathbf{e}_R \cdot \nabla m)_P (\mathbf{e}_R \cdot \nabla m)_{P'} \rangle = \frac{1}{2} \left(\frac{\partial^2 D}{\partial \eta^2} \cos \phi' + \frac{\partial^2 D}{\partial \eta \partial \xi} \sin \phi' \right). \quad (6.4)$$

(vi) Velocity and temperature fluctuations at scales of order R are nearly uncorrelated. The temperature and velocity fields of large-scale eddies can be highly correlated, especially in a thermally driven boundary layer, but the correlation is lost in the cascade to finer scales. According to (2.4), therefore,

$$D = \frac{1}{\sigma_0^2} \langle \{(u_1)_{P'} - (u_1)_P\}^2 \rangle + \frac{1}{4T_0^2} \langle \{\theta_{P'} - \theta_P\}^2 \rangle,$$

a sum of non-interacting inertial and thermal contributions.

That completes the list of approximations that simplify the original integral (6.1). All of them are realistic; the most questionable is probably the assumption (vi) of inertial and thermal independence (Tatarski 1961, p. 194). One consequence of the local isotropy condition (iii) remains to be exploited. Suppose that axial structure functions for the random fields u_1 and θ are defined as follows:

$$D_u(\sigma, x) = \langle \{u_1(x + \sigma) - u_1(x)\}_A^2 \rangle,$$

$$D_\theta(\sigma, x) = \langle \{\theta(x + \sigma) - \theta(x)\}_A^2 \rangle,$$

where the remaining arguments x_2 and x_3 are zero (or constant). Then local isotropy (iii) and independence (vi) imply that

$$D = \frac{1}{\sigma_0^2} \left(\frac{\eta^2 + \zeta^2}{2\sigma} D'_u + D_u \right) + \frac{1}{4T_0^2} D_\theta. \quad (6.5)$$

The origin of the thermal term is obvious, and the first term comes from a standard relation in the theory of solenoidal, statistically isotropic vector fields (Batchelor 1953, p. 46). The prime here and from now on represents differentiation with respect to the scalar σ . Condition (iv), which has not yet been used, results in the following geometrical relations valid on the local cylindrical sleeve:

$$\sin \phi' = \zeta/R, \quad \cos \phi' = 1 + \eta/R, \quad \zeta^2 = -2R\eta - \eta^2 \quad (6.6)$$

(note from figure 12 that $-2R \leq \eta \leq 0$). Equations (6.2)–(6.6), after some straightforward algebra, give rise to the following expression for the mean-square fractional pressure perturbation, exclusive of the phase shift:

$$\begin{aligned} \langle \psi^2(t) \rangle &= \frac{1}{4\pi} \int_0^\infty dx (x^2/R^3) \iint_{\text{cyl.}} dA \left\{ \frac{1}{\sigma_0^2} [(R\eta/\sigma^2 + 4\eta^2/\sigma^2 + 3R\eta^3/\sigma^4) \right. \\ &\quad \times (D'_u/\sigma - D''_u) + (\eta^3/\sigma^3) R D''_u + 2(1 + \eta/R) D'_u/\sigma] \\ &\quad \left. + \frac{1}{4T_0^2} [(\eta^2/\sigma^2) (D'_\theta/\sigma - D''_\theta) + (1 + \eta/R) D'_\theta/\sigma] \right\}. \end{aligned} \quad (6.7)$$

The square brackets here and in subsequent equations no longer indicate retarded times. As complicated as it appears, the surface integral over the cylindrical sleeve can be evaluated analytically for structure functions D_u and D_θ of the Kolmogorov form.

7. Scattering in the Kolmogorov inertial subrange

The Kolmogorov length l , which characterizes the finest eddies in a body of turbulence, is typically a fraction of an inch in the atmospheric boundary layer (Lumley & Panofsky 1964, p. 82). In a boundary layer of height δ , the radius R of the paraboloid of dependence is typically $(2h\delta)^{1/2}$. R can be as small as l , therefore, only if $h \sim (l/\delta)l$, an absurdly small distance between the shock and the observation point. The case $R \ll l$ is investigated in § 8 for the sake of mathematical completeness, but it is clear that $R \gg l$ for all meaningful values of h . That fact, in conjunction with the argument of § 6, means that R satisfies the double inequality

$$L \gg R \gg l$$

and lies squarely within the inertial subrange. For σ comparable to such values of R , Kolmogorov's similarity theory and much experimental evidence lead to the following expressions for the structure functions D_u and D_θ (Tatarski 1961, pp. 27-51):

$$\left. \begin{aligned} D_u(\sigma, x) &= K_u \epsilon_u(x)^{2/3} \sigma^{2/3}, \\ D_\theta(\sigma, x) &= K_\theta \epsilon_\theta(x) \epsilon_u(x)^{-1/3} \sigma^{2/3}. \end{aligned} \right\} \quad (7.1)$$

ϵ_u is the mean rate of dissipation of turbulent kinetic energy $\frac{1}{2}\langle \mathbf{u}^2 \rangle$ by viscous stress, and ϵ_θ is the mean rate of destruction of the analogous thermal quantity $\frac{1}{2}\langle \theta^2 \rangle$ by conduction. The dimensionless quantities K_u and K_θ are generally supposed to be universal constants, though argument persists regarding both their magnitude and their universality. K_u equals $(1.315\dots)\gamma$, where γ is the constant of proportionality in the famous $k^{-5/3}$ law for the turbulent energy spectrum (Ellison 1962). The best experimental results available (Grant, Stewart & Moilliet 1962) indicate that $\gamma \approx 1.44$. Tatarski (1961, p. 194) finds that $K_\theta \approx 5.76$. The estimates

$$K_u \approx 1.9, \quad K_\theta \approx 5.8 \quad (7.2)$$

represent a fair summary of what little experimental evidence is available about the constants of proportionality in (7.1). The value $\frac{2}{3}$ of the exponents of σ has been confirmed quite accurately, by contrast, and that is the only piece of information essential to the following analysis.

The surface integral in (6.7) can easily be shown to converge for the structure functions (7.1), both as $\sigma/R \rightarrow \infty$ and as $\sigma/R \rightarrow 0$ (provided $R > 0$; cf. § 8). Its convergence in the limit $\sigma/R \rightarrow \infty$, in fact, constitutes the proof that eddies of scale R really are responsible for scattering in atmospheric turbulence. If the surface integral had failed to converge as $\sigma/R \rightarrow \infty$, then the large-scale eddies would have entered the problem of evaluating $\langle \psi^2(t) \rangle$, and no universal expression of the kind about to be derived could have been found. If it had failed to converge as $\sigma/R \rightarrow 0$, then viscosity and conductivity would have had to be introduced explicitly to provide cut-offs around $\sigma = 0$ (cf. equation (8.4)). Since the

surface integral does converge in terms of (7.1), it is obviously proportional to $R^2R^{-\frac{1}{2}}$. The complete integrand of the integral over x in (6.7) is therefore proportional to $(x^2/R^3)R^2R^{-\frac{1}{2}}$, which equals $x^{\frac{1}{2}}(2h)^{-\frac{7}{2}}$ by virtue of (3.2). It follows at once that

$$\langle \psi'^2(t) \rangle = \frac{1}{h^{\frac{7}{2}}} \int_0^\infty x^{\frac{1}{2}} \left(A_u K_u \frac{e_u^{\frac{3}{2}}}{c_0^2} + A_\theta K_\theta \frac{e_\theta e_u^{-\frac{1}{2}}}{4T_0^2} \right) dx, \tag{7.3}$$

where A_u and A_θ are dimensionless constants depending on the details of (6.7). By substituting (7.1) into (6.7), one arrives at the following expressions for A_u and A_θ :

$$\left. \begin{aligned} A_u &= \frac{1}{3\pi 2^{\frac{7}{2}}} \iint_{\text{unit cyl.}} \left[(1 + \eta) + \frac{2}{9} \frac{\eta^3}{\sigma^4} + \frac{2}{3} \left(\frac{\eta}{\sigma^2} + 4 \frac{\eta^2}{\sigma^2} + 3 \frac{\eta^3}{\sigma^4} \right) \right] \frac{dA}{\sigma^{\frac{1}{2}}}, \\ A_\theta &= \frac{1}{6\pi 2^{\frac{7}{2}}} \iint_{\text{unit cyl.}} \left[(1 + \eta) + \frac{4}{3} \frac{\eta^2}{\sigma^2} \right] \frac{dA}{\sigma^{\frac{1}{2}}}. \end{aligned} \right\} \tag{7.4}$$

The area element dA and the variables η and σ have been scaled on the radius R , so the integrands in (7.4) are dimensionless, and the radius of the cylindrical sleeve over which the integrations are to be performed is unity.

Because of the simple geometry of the unit cylinder, the expressions (7.4) can be evaluated without recourse to numerical integration. According to the geometrical relations (6.6),

$$\eta = \cos \phi' - 1,$$

and

$$\sigma^2 = \xi^2 + \eta^2 + \zeta^2 = \xi^2 - 2\eta,$$

for a point on the unit cylinder. Thus σ and η can be eliminated from (7.4) in favour of ξ and ϕ' . The area element dA can be written as $d\xi d\phi'$. It is then straightforward to perform the integration over ξ from $-\infty$ to ∞ for fixed ϕ' and to integrate that result over ϕ' . The final results are as follows:

$$\left. \begin{aligned} A_u &= \frac{55}{54} \left\{ \left(\frac{2}{\pi} \right)^{\frac{1}{2}} \frac{\Gamma(\frac{3}{2}) \Gamma(\frac{5}{6}) \Gamma(\frac{4}{3})}{\Gamma(\frac{5}{3}) \Gamma(\frac{11}{6})} \right\} = 0.702\dots, \\ A_\theta &= \frac{5}{9} \left\{ \left(\frac{2}{\pi} \right)^{\frac{1}{2}} \frac{\Gamma(\frac{3}{2}) \Gamma(\frac{5}{6}) \Gamma(\frac{4}{3})}{\Gamma(\frac{5}{3}) \Gamma(\frac{11}{6})} \right\} = 0.383\dots \end{aligned} \right\} \tag{7.5}$$

That completes the analytical solution for the mean-square pressure perturbation due to scattering in the inertial subrange. Since (7.3) is valid for all meaningful values of h , it is correct to say that the inertial subrange of atmospheric turbulence is fully responsible for the fine structure of sonic bangs. Notice that the mathematical difference between inertial and thermal scattering, which appears considerable at the level of (6.5), has been reduced in (7.5) to the difference between $\frac{5.5}{5.4}$ and $\frac{5}{9}$.

It is interesting that Tatarski (1961, pp. 164–172) obtained a solution formally similar to (7.3) for the problem of scattering from a periodic electromagnetic or acoustic wave. Tatarski's equation (8.17) describes the mean-square amplitude fluctuations, observed at the ground, of a sinusoidal wave propagating down through a turbulent atmosphere. The wavelength λ of the wave must satisfy the same conditions that h satisfies here (i.e. $L \gg (\lambda\delta)^{\frac{1}{2}} \gg l$) but in addition must be small compared with l . Tatarski used Fourier analysis rather than the concept

of the paraboloid of dependence. He did not handle inertial scattering correctly (cf. Kraichnan's appendix to Tatarski's book), but the error appears not to have affected the qualitative structure of his answer. Apart from numerical coefficients, Tatarski's result differs from (7.3) only in the appearance of a factor k^2 , involving the wave-number k of the incident sound, in place of the factor h^{-2} . The correspondence can be understood readily by applying the general solution (3.12) to a high-pitched sinusoidal wave (Crow 1968, § 8).

Equation (7.3) assumes a more serviceable form when the integral along the x -axis normal to the shock is transformed into an integral over altitude y . The vertex angle of the Mach cone shown in figure 1 is $\sin^{-1}(1/M)$ for an aircraft travelling at Mach number M , so $x(y) = [M/(M^2 - 1)^{1/2}]y$ for an observation point directly under the flight path of the aircraft. It follows from (7.2) to (7.5) that

$$\langle \psi^2(t) \rangle = (t_c/t)^{7/2}, \quad \left. \begin{array}{l} \text{for a critical time} \\ t_c = \frac{1}{c_0} \left[\frac{M}{(M^2 - 1)^{1/2}} \right]^{11/7} \left[\int_0^\infty y^{5/2} \left(1.33 \frac{c_u^{3/2}}{c_0^2} + 0.55 \frac{c_\theta c_u^{-1/2}}{T_0^2} \right) dy \right]^{2/7} \end{array} \right\} \quad (7.6)$$

All information, regarding both flight and weather conditions, needed to predict the intensity of sonic-bang distortions is bound in the single parameter t_c . When $t = t_c$, the root-mean-square pressure perturbation is unity, or rather would be unity if first-order theory were valid in the highly perturbed region near the shock.

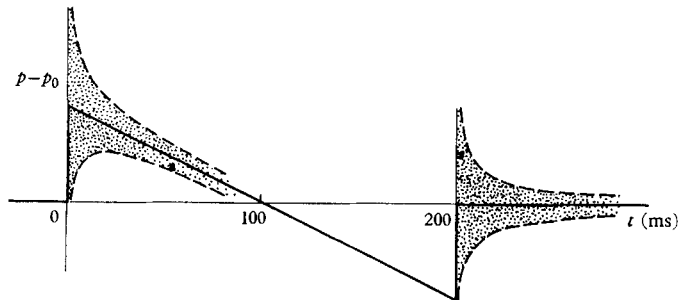


FIGURE 13. Variance of a 200 ms N -wave under conditions such that $t_c = 2$ ms.

Figure 13 illustrates the amplitude of the distortions that would be expected on an N -wave of 200 ms duration if t_c were 2 ms. The solid line is the basic wave-form $p^N(t)$, and the dashed lines are $p^N(t)$ plus and minus the root-mean-square perturbation $\Delta p (t_c/t)^{7/2}$, where t is the time elapsed since the passage of the nearest shock. The shaded band is the region of probable occupancy for pressure histories recorded under conditions such that $t_c = 2$ ms. Notice that the apparent duration of the region of significant perturbation behind a shock is 20–30 t_c , much larger than t_c itself. A comparison between figures 3 and 13 suggests that 2 ms is probably as large a value of t_c as is likely to be encountered under routine meteorological conditions. Values of t_c between 0.5 and 1.5 ms are probably typical. These remarks are tentative, of course, since there have not yet been sufficient data taken under identical meteorological conditions to permit a meaningful experimental evaluation of the ensemble average $\langle \psi^2(t) \rangle$.

In order to get some idea of the theoretical magnitude of t_c , let us suppose that thermal scattering is insignificant and that the atmospheric boundary layer behaves exactly like a wind-tunnel boundary layer under a uniform free stream. The assumption that thermal scattering is negligible has some justification from the last paragraph of § 2. The assumption about the structure of the atmospheric boundary layer is highly questionable, but it permits the dissipation function ϵ_u to be written in a universal form, namely

$$\epsilon_u = u_*^3 \delta^{-1} W(y/\delta), \quad (7.7)$$

involving the skin-friction velocity u_* (square-root of the ratio of wall stress to density), the altitude δ where the mean wind speed is 99.5 % of its free-stream value, and a universal function W known from wind-tunnel data. Thus

$$y^{\frac{3}{2}} \epsilon_u^{\frac{2}{3}} = u_*^2 \delta^{\frac{1}{2}} F(y/\delta)$$

for another known function F . According to (7.6), $F(y/\delta)$ is a measure of the scattering efficacy of a turbulent layer of unit thickness at altitude y . F is plotted as a solid line in figure 14 for the case of a wind-driven boundary layer under zero

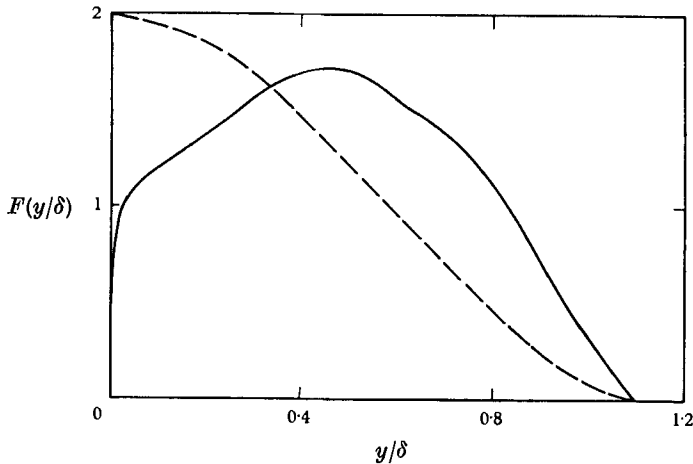


FIGURE 14. Scattering efficacy in a wind-driven boundary layer. The solid line represents scattering efficacy, and the dashed line represents Reynolds stress normalized on $\frac{1}{2}u_*^2$. δ is the altitude at which the wind speed is 99.5 % of its free-stream value.

pressure gradient. Data for the plot are taken from Bradshaw, Ferriss & Atwell (1967); there is some uncertainty about the value of F in the outer 20 % of the boundary layer, enough to cause a 10 % uncertainty in the area of the plot. The Reynolds stress, normalized on $\frac{1}{2}u_*^2$ for visual convenience, is plotted in the same figure as a dashed line. F is seen to be much more uniform across the boundary layer than the Reynolds stress. The combination of a decreasing $\epsilon_u^{\frac{2}{3}}$ and an increasing geometrical weighting factor $y^{\frac{3}{2}}$ makes all strata of the boundary layer about equally effective as sources of scattered waves. The area under the plot of F is 1.3. Thus

$$\int_0^\infty y^{\frac{3}{2}} \epsilon_u^{\frac{2}{3}} dy = 1.3 u_*^2 \delta^{\frac{5}{2}},$$

and, according to (7.6),

$$t_c = 1.6 \left[\frac{M}{(M^2 - 1)^{\frac{1}{2}}} \right]^{\frac{1}{7}} \left(\frac{u_*}{c_0} \right)^{\frac{1}{7}} \left(\frac{\delta}{c_0} \right), \quad (7.8)$$

for the simplified boundary-layer model under consideration. Equation (7.8) implies that the root-mean-square perturbation is proportional to the turbulent Mach number u_*/c_0 and that t_c is proportional to the time δ/c_0 required for an acoustic wave to travel the height of the boundary layer. Suppose that

$$M = 2, \quad u_*/c_0 = 0.005, \quad \delta = 3000 \text{ ft.} \quad (7.9)$$

The values of u_* and δ chosen in (7.9) are probably as large as could be expected in a wind-driven boundary layer. It follows from (7.8) and (7.9) that

$$t_c = 0.69 \text{ ms,}$$

a figure consistent with the values of 0.5–1.5 ms implicit in experimental data of the sort shown in figure 3. Estimates of t_c based on this model should, if anything, be low, since thermal convection is likely to be a major source of turbulent kinetic energy in the outer part of an atmospheric boundary layer.

The critical time t_c is an index of sonic-bang irregularities, potentially a criterion for deciding whether a supersonic airliner should be allowed to pass over a city under given weather conditions. But the weather conditions involved in (7.6) and, for that matter, in (7.8) are not subject to routine measurement. Very little systematic information about $\epsilon_u(y)$ exists beyond that contained in (7.8), and even less is known about $\epsilon_\theta(y)$. There is nevertheless reason to hope that the required information will become available in a decade or so. Numerical weather-prediction schemes, currently under vigorous development, must calculate the large-scale motion of the atmosphere. The large-scale flow depends strongly on the turbulent transport of momentum and heat through the boundary layer, and those transport rates in turn are coupled to the rates of dissipation. The dissipation functions $\epsilon_u(y)$ and $\epsilon_\theta(y)$ act as relaxation terms in the equations for the transport rates (Bradshaw *et al.* 1967; Zilitinkevich *et al.* 1967). Any successful weather-prediction scheme will probably have to carry the dissipation functions along in the computations. By the time supersonic air travel becomes commonplace, estimates of t_c may be obtainable as by-products of weather forecasts.

8. Perturbation and disintegration of shock fronts

The quantity $\psi(0)$ is the fractional pressure perturbation just behind an ideally discontinuous shock. The abstract character of $\psi(0)$ should be borne in mind through the analysis that follows (especially because $\langle \psi^2(0) \rangle$ turns out to be unconscionably large). Equation (4.2) gives the first-order contribution to $\psi(0)$, but (4.2) rests on the limit $R/l \rightarrow 0$, which makes sense for a mathematical discontinuity but not necessarily for a real shock of finite thickness. At the base of the atmospheric boundary layer, $\psi(h/c_0)$ converges onto $\psi(0)$ only for distances h incomparably smaller than the normal thickness of an N -wave shock.

Whatever its physical interpretation, the mean-square quantity $\langle \psi^2(0) \rangle$ can

be derived by taking a rather subtle limit of (6.7) as $R/l \rightarrow 0$ or, more straightforwardly, by squaring and averaging (4.2) under assumptions (i)–(vi) of § 6:

$$\langle \psi^2(0) \rangle = \int_0^\infty dx \int_0^\infty d\sigma x^2 \left[\frac{6}{c_0^2} \left(\frac{D'_u}{\sigma^3} - \frac{D''_u}{\sigma^2} \right) + \frac{2}{4T_0^2} \left(\frac{D'_\theta}{\sigma^3} - \frac{D''_\theta}{\sigma^2} \right) \right]. \tag{8.1}$$

According to (7.6), the mean-square perturbation $\langle \psi^2(t) \rangle$ grows without limit as $t \rightarrow 0$ for the particular choice (7.1) of the structure functions, so it comes as no surprise that (8.1) diverges as $\sigma \rightarrow 0$ for the same structure functions. The divergence is artificial, however, because equations (7.1) are invalid for $\sigma < l$. The equations of motion and heat flow imply instead that

$$\left. \begin{aligned} D_u(\sigma, x) &= \frac{\epsilon_u(x)}{15\nu} \sigma^2, \\ D_\theta(\sigma, x) &= \frac{\epsilon_\theta(x)}{3\kappa} \sigma^2, \end{aligned} \right\} \tag{8.2}$$

for $\sigma \ll l$, where ν is the viscosity and κ is the conductivity of the fluid (Tatarski 1961, pp. 27–51). The transition from (8.2) to (7.1) takes place around $\sigma \sim l$, since the Kolmogorov length l is defined as $(\nu^3/\epsilon_u)^{1/4}$. Equation (7.6) could hold right up to the shock only if the rate of energy dissipation were infinite.

The integral over σ in (8.1) obviously converges in the limit $\sigma \rightarrow 0$ for any structure functions that vary as σ^2 . Equations (8.2) cannot be substituted directly into (8.1), however, because the resulting integral would diverge as $\sigma \rightarrow \infty$. Equations (7.1) allow the integral to converge as $\sigma \rightarrow \infty$ but cause it to diverge as $\sigma \rightarrow 0$. Thus the viscous subrange, in which (8.2) is valid, and the inertial subrange, represented by (7.1), both contribute to $\langle \psi^2(0) \rangle$, and the behaviour of the structure functions in both limits $\sigma \ll l$ and $\sigma \gg l$ must be taken into account in (8.1) in order for the integral to converge. There is no deductive theory that bridges the gap between (7.1) and (8.2), but it suffices here to adopt a simple interpolation formula:

$$D_a = \frac{\alpha_a \sigma^2}{(1 + \beta_a \sigma^2)^{3/2}}. \tag{8.3}$$

The subscript a stands for u or θ . Formula (8.3) reproduces both (7.1) and (8.2) in the appropriate limits, provided that

$$\begin{aligned} \alpha_u &= \frac{\epsilon_u}{15\nu}, & \alpha_\theta &= \frac{\epsilon_\theta}{3\kappa}, \\ \beta_u &= \frac{\epsilon_u^{1/2}}{(15\nu K_u)^{3/2}}, & \beta_\theta &= \frac{\epsilon_\theta^{1/2}}{(3\kappa K_\theta)^{3/2}}. \end{aligned}$$

Actual structure functions could hardly deviate far from (8.3). The integrals over σ can easily be evaluated now, since it follows from (8.3) that

$$\int_0^\infty \left(\frac{D'_a}{\sigma^3} - \frac{D''_a}{\sigma^2} \right) d\sigma = \alpha_a \beta_a^{1/2} \left(\frac{\Gamma(\frac{3}{2}) \Gamma(\frac{7}{6})}{\Gamma(\frac{5}{3})} \right).$$

Thus
$$\langle \psi^2(0) \rangle = \int_0^\infty x^2 \left(\frac{C_u}{K_u^{3/2}} \frac{\epsilon_u^{3/2}}{c_0^2 \nu^{3/2}} + \frac{C_\theta}{K_\theta^{3/2}} \frac{\epsilon_\theta \epsilon_u^{1/2}}{4T_0^2 \kappa^{1/2}} \right) dx, \tag{8.4}$$

where

$$\left. \begin{aligned} C_u &= \frac{2}{5(15)^{\frac{3}{4}}} \left\{ \frac{\Gamma(\frac{3}{2})\Gamma(\frac{7}{6})}{\Gamma(\frac{5}{3})} \right\} = 0.047\dots, \\ C_\theta &= \frac{2}{(3)^{\frac{7}{4}}} \left\{ \frac{\Gamma(\frac{3}{2})\Gamma(\frac{7}{6})}{\Gamma(\frac{5}{3})} \right\} = 0.266\dots \end{aligned} \right\} \quad (8.5)$$

Equations (8.4) and (8.5) are the analogues of (7.3) and (7.5) in the foregoing section. The analogue of (7.6), involving an integral over altitude y and incorporating the experimental values (7.2) for the supposedly universal constants K_u and K_θ , is as follows:

$$\langle \psi^2(0) \rangle = \left[\frac{M}{(M^2 - 1)^{\frac{1}{2}}} \right]^3 \int_0^\infty y^2 \left(0.029 \frac{\epsilon_u^{\frac{5}{4}}}{c_0^2 \nu^{\frac{1}{4}}} + 0.018 \frac{\epsilon_\theta \epsilon_u^{\frac{1}{4}}}{T_0^2 \kappa^{\frac{1}{4}}} \right) dy. \quad (8.6)$$

The model atmospheric boundary layer introduced in §7 can be used again to estimate the order of magnitude of (8.6). According to (7.7),

$$y^2 \epsilon_u^{\frac{5}{4}} = u_*^{\frac{5}{4}} \delta^{\frac{3}{4}} G(y/\delta),$$

where G is another universal function related to the dissipation function W , which in turn is known from wind-tunnel experiments. In the co-ordinates of figure 14, G is shaped roughly like a symmetrical pyramid, with a base running from $y/\delta = 0$ to 1, and with a sharp maximum of 2.0 at $y/\delta = 0.5$. The area under the curve $G(y/\delta)$ is 1.17, so

$$\langle \psi^2(0) \rangle = 0.034 \left[\frac{M}{(M^2 - 1)^{\frac{1}{2}}} \right]^3 \left(\frac{u_*}{c_0} \right)^2 \left(\frac{u_* \delta}{\nu} \right)^{\frac{7}{4}} \quad (8.7)$$

for the idealized model, in the absence of thermal scattering. Equation (8.7) states that the mean-square pressure perturbation just behind a mathematically discontinuous shock is proportional to the square of the eddy Mach number u_*/c_0 , a very small quantity, but that it is also proportional to the seven-fourths power of the Reynolds number $u_*\delta/\nu$ based on the skin-friction velocity and the boundary-layer thickness. For an atmospheric boundary layer, $u_*\delta/\nu$ is tremendous ($\nu \approx 1.3 \times 10^{-4}$ ft.²/s). Under the conditions specified in (7.9), equation (8.7) implies that

$$\langle \psi^2(0) \rangle = 1.5 \times 10^8,$$

a prediction that conveys no physical meaning, other than a suggestion that the region immediately behind a shock is likely to be very much disturbed by scattered waves under almost any atmospheric conditions. The first-order pressure perturbation inside a real shock of finite thickness would have to be calculated from the superposition integral in the general solution (3.12). Presumably the integration would smooth the extremely sharp perturbations suggested by (8.6) down to more reasonable values.

N -wave perturbations do attain their largest values in the vicinity of the shocks (figure 3), in qualitative accord with the foregoing analysis. Apart from these extreme amplitude fluctuations, the most striking feature of N -wave shocks is that they are about 1000 times thicker than molecular viscosity alone would lead one to expect (Lilley 1965). Of course the very considerable thickening shown in figure 3(b) is a manifestation of an inverted shock spike ($\psi(0) < 0$), but even

peaked shocks are 1–5 ft. thick, whereas the Taylor thickness of a 2 lb./ft.² shock is 1.5×10^{-3} ft. (Lighthill 1956, p. 289). Relaxation processes other than molecular diffusion may operate (e.g. transfer of energy from translational to vibrational degrees of molecular freedom), but none seems likely to explain the observations. A process having a relaxation time t_r may give rise to a shock thickness of order $c_0 t_r$, corresponding to a recorded rise time of t_r , but no molecular process is available having a relaxation time comparable to the 1–5 ms rise times that are observed.

Turbulence evidently must be invoked to explain the thickening of shocks as well as the pressure spikes behind them. A naive eddy-viscosity argument is surely illegitimate: turbulence acts as a viscous medium with respect to a long, low-frequency wave (Crow 1967), but a short, sudden wave is at issue here. Various alternative explanations come to mind, but the only one that bears careful analysis is that shock thickening and scattering are connected. The acoustic energy in the trail of scattered waves comes from somewhere, and the obvious possibility is that it is beaten out of the shock front by the intense interactions that give rise to scattering. In the case of thermal interactions, the shock front is the *only* possible source of acoustic energy. Eddies might supply part of the energy arising out of inertial interactions, but the symmetry between the inertial and thermal forcing terms in (2.1) suggests that eddies should no more supply energy than passive thermal fluctuations do. According to (7.6), the energy density of the scattered waves trails off as $(c_0 t_c/h)^2$ behind the shock (h is being interpreted here as distance behind the shock at a fixed time, although it was introduced as $c_0 t$ in §3; the distinction is immaterial as long as $h \ll \delta$). That energy density is integrable provided h is given a lower bound, and the appropriate lower bound is the shock thickness. If the energy of the scattered waves drains from the shock front, it follows that the shock must thicken an amount $\sim c_0 t_c$, which has just the right order of magnitude to explain the observations. *The critical time t_c acts as the relaxation time for the process of shock thickening.* The physical picture that emerges is that the shock front disintegrates under concentrated interaction with turbulence, leaving a trail of deflected fragments which show up as the perturbations treated by first-order scattering theory.

An obvious question can be raised against this idea: why does shock thickening not appear in (3.8) as a term having a non-zero mean? The answer follows from the energy-balance argument above: shock thickening is a second-order effect and cannot appear in a first-order scattering theory. Acoustic scattering theory is basically a means of finding successive terms in a perturbation expansion of $p(\mathbf{x}, t) - p_0$ in powers of a typical value, m_* say, of the scattering field $m(\mathbf{x}, t)$. For a shock,

$$p(\mathbf{x}, t) - p_0 = \Delta p \{H(x + c_0 t) + m_* S_1(\mathbf{x}, t) + m_*^2 S_2(\mathbf{x}, t) + O(m_*^3)\},$$

in the usual co-ordinates. The combination $m_* S_1(\mathbf{x}, t)$ was called $s(\mathbf{x}, t)$ in §§2–3 and is the subject of first-order theory. The quantity $S_2(\mathbf{x}, t)$, which would be given by a second-order theory, depends quadratically on the scattering field and presumably has a non-zero mean. The mean energy E^S scattered per unit

area of shock therefore contains $O(m_*^2)$ contributions from both $\langle S_1^2 \rangle$ and $\langle HS_2 \rangle$:

$$E^S = \frac{(\Delta p)^2}{\rho_0 c_0^2} \left\{ m_*^2 \int_{-t/c_0}^{\infty} (\langle S_1^2(\mathbf{x}, t) \rangle + \langle S_2(\mathbf{x}, t) \rangle_A) dx + O(m_*^3) \right\}.$$

If the argument is correct that scattering leaves the net acoustic energy unchanged (at least to $O(m_*^2)$), then the integral along the x -axis must be zero. Since $\langle S_1^2 \rangle$ is positive, $\langle S_2 \rangle$ must be mainly negative, which is what one would expect of an $\langle S_2 \rangle$ representing shock thickening.†

Acoustic scattering theory is a rather delicate affair even to first order (Batchelor 1957), so a second-order theory might require a much deeper analysis of the interaction between sound and turbulence than has been conducted so far. Since shock thickening appears to be a result of second-order scattering, on the other hand, the technological rewards of such an analysis would be very great and should serve as a stimulus.

REFERENCES

- BATCHELOR, G. K. 1953 *The Theory of Homogeneous Turbulence*. Cambridge University Press.
- BATCHELOR, G. K. 1957 Wave scattering due to turbulence. *Symposium on Naval Hydrodynamics*, ch. XVI, publication 515, National Academy of Science—National Research Council. Washington, D.C.
- BRADSHAW, P., FERRISS, D. H. & ATWELL, N. P. 1967 Calculation of boundary-layer development using the turbulent energy equation. *J. Fluid Mech.* **28**, 593.
- CARLSON, H. W. 1967 Experimental and analytical research on sonic boom generation at NASA. *Sonic Boom Research*. NASA SP-147.
- CHERNOV, L. A. 1960 *Wave Propagation in a Random Medium*. New York: McGraw-Hill.
- COURANT, R. & HILBERT, D. 1965 *Methods of Mathematical Physics*, vol. II. New York: Interscience.
- CROW, S. C. 1967 Visco-elastic character of fine-grained isotropic turbulence. *Phys. Fluids*, **10**, 1587.
- CROW, S. C. 1968 Distortion of sonic bangs by atmospheric turbulence. *NPL Aero Report* 1260.
- ELLISON, T. H. 1962 The universal small-scale spectrum of turbulence at high Reynolds number. *Mecanique de la Turbulence*. Paris: CNRS.
- FRIEDMAN, M. P., KANE, E. J. & SIGALLA, A. 1963 Effects of atmosphere and aircraft motion on the location and intensity of a sonic boom. *AIAA J.* **1**, 1327.
- GARRICK, I. E. & MAGLIERI, D. J. 1968 A summary of results on sonic-boom pressure-signature variations associated with atmospheric conditions. *NASA TN D-4588*.
- GRANT, H. L., STEWART, R. W. & MOILLIET, A. 1962 Turbulence spectra from a tidal channel. *J. Fluid Mech.* **12**, 241.
- JOHNSON, D. R. & ROBINSON, D. W. 1967 The subjective evaluation of sonic bangs. *Acustica*, **18**, 241.
- KANE, E. J. & PALMER, T. Y. 1964 Meteorological aspects of the sonic boom. *Boeing SRDS Report* no. RD 64-160.

† The mean energy spectrum of first-order N -wave perturbations was calculated in the earlier version of this paper (Crow 1968). The result was added to the spectrum of the incident N -wave after an *ad hoc* correction for thickening had been made. That procedure does not seem enlightening now that thickening and scattering are being regarded as aspects of the same phenomenon, so the spectrum analysis is not included here.

- LANSING, D. L. 1964 Application of acoustic theory to prediction of sonic-boom ground patterns from maneuvering aircraft. *NASA TN D-1860*.
- LIGHTHILL, M. J. 1953 Interaction of turbulence with sound or shock waves. *Proc. Camb. Phil. Soc.* **49**, 531.
- LIGHTHILL, M. J. 1956 Viscosity effects in sound waves of finite amplitude. *Surveys in Mechanics*. Cambridge University Press.
- LILLEY, G. M. 1965 The structure of shock waves at large distances from bodies travelling at high speeds. *Rapports du 5^e Congres International d'Acoustique*, vol. II. Liege.
- LUMLEY, J. L. & PANOFSKY, H. A. 1964 *The Structure of Atmospheric Turbulence*. New York: Interscience.
- PHILLIPS, H. B. 1933 *Vector Analysis*. New York: John Wiley.
- TATARSKI, V. I. 1961 *Wave Propagation in a Turbulent Medium*. New York: McGraw-Hill.
- TOWNSEND, A. A. 1957 Turbulent flow in a stably stratified medium. *J. Fluid Mech.* **3**, 261.
- WARREN, C. H. E. 1965 The propagation of sonic bangs in a non-homogeneous still atmosphere. *Aero. Res. Council Report* no. 26774.
- WEBB, D. R. B. & WARREN, C. H. E. 1965 Physical characteristics of the sonic bangs and other events at Exercise Westminster. *Royal Aircraft Establishment Tech. Rep.* no. 65248.
- WHITHAM, G. B. 1952 The flow pattern of a supersonic projectile. *Comm. on Pure and Appl. Math.* **5**, 301.
- WHITHAM, G. B. 1956 On the propagation of weak shock waves. *J. Fluid Mech.* **1**, 290.
- ZILITINKEVICH, S. S., LAIKTMAN, D. L. & MONIN, A. S. 1967 Dynamics of the atmospheric boundary layer. *Izv., Atmos. Oceanic Phys.* **3**, 170.